In-situ thermal conductivity of sorption composites: An analytical approach

By:

Amin Shafiepour

B.Sc., University of Tehran, 2019

Thesis Submitted in Partial Fulfillment of the
Requirements for the Degree of
Master of Applied Science

in the
School of Mechatronic Systems Engineering
Faculty of Applied Sciences

SIMON FRASER UNIVERSITY
Summer 2021

Declaration of Committee

Name:	**Amin Shafiepour**
Degree:	**Master of Applied Science**
Title:	**In-situ thermal conductivity of sorption composites: An analytical approach**
Committee:	**Chair:** **Helen Bailey** Lecturer, Mechatronic Systems Engineering
	Majid Bahrami Supervisor Professor, Mechatronic Systems Engineering
	Sami Khan Committee Member Assistant Professor, Sustainable Energy Engineering
	Byron Gates Examiner Professor, Chemistry

Abstract

A new analytical quasi-steady-state model to estimate the effective thermal conductivity and diffusivity of wetted sorbent composites containing thermally-conductive additives is developed based on the effective medium theory, or unit cell approach, and covers all salient morphological parameters, material properties, and operating conditions. The proposed closed-form solution is validated with experimental data using several consolidated salt-in-matrix sorbents with silica gel, $CaCl_2$, polyvinyl alcohol (PVA) binder, and 0-15 wt.% of graphite flakes (GF), as well as 1-5 wt.% of expanded natural graphite (ENG) as thermally-conductive additives fabricated and characterized in our lab. The addition of 15wt.% of GF, and 5 wt.% of ENG to the composite sorbent when tested with a relative humidity (RH) of 2%, resulted in a ~ 536%, and a ~ 572% enhancement in the effective thermal conductivity. Also, increasing the sorbed water content in the composite with no thermally-conductive additives from 0.02 to 0.9 $g \cdot g^{-1}$ caused a 318% increase in the thermal conductivity.

Keywords: functional composites, sorption system, heat and mass transfer, thermal conductivity, natural graphite, thermal diffusivity; and analytical modeling

To my wonderful loving family,

for all their support and dedication

Acknowledgements

I would like to express my sincere gratitude towards many people who made accomplishing this dissertation possible. I am thankful to my Senior Supervisor, Professor Majid Bahrami, for his great support and guidance throughout my Master's studies. I'm also thankful to my colleagues and friends at the Laboratory for Alternative Energy Conversion (LAEC) at Simon Fraser University (SFU), especially to Postdoctoral Fellows, Drs. Hesam Bahrehmand, and Claire McCague, for their technical support and helpful suggestions.

My appreciation extends to my Supervisory Committee Members, Drs. Byron Gates and Sami Khan for their time, discussions, and beneficial comments on my research project. I am also grateful to Dr. Helen Bailey for accepting to be my Defense Committee Chair.

I would like to gratefully acknowledge the financial support of Innovative BC and the Natural Sciences and Engineering Research Council of Canada (NSERC) through the Collaborative Research and Development Grant (CRDPJ 488777-15).

Finally, I am genuinely thankful to my beloved parents and my best friends who have always been there for me with their patience, love, and support.

Table of Contents

List of Tables

List of Figures

Nomenclature

k	Thermal conductivity, $W \cdot m^{-1} \cdot K^{-1}$
R	Thermal resistance, $K \cdot W^{-1}$
T	Temperature, K
$\dot{Q}$	Heat flow rate, W
t	Thickness, m
r	Radius, m
L	Unit cell length, m
u	Uncertainty
d_p	Pore size diameter, m
d_c	Equivalent cubic diagonal, m
a	Side length of consolidated unit cell, m

Greek symbols

α	Thermal diffusivity, $m^2 \cdot s^{-1}$
ω	Water uptake, $g \cdot g^{-1}$
ε	Porosity
ρ	Density, $kg \cdot m^{-3}$
θ	Angle, degree
φ	Additive weight percentage

Subscripts

eff	Effective
m	Medium
p	Additive particle
s	Solid host matrix
w	Water

Abbreviations

TPS	Transient plane source

RH	Relative humidity
ENG	Expanded natural graphite
GF	Graphite flakes
PVA	Polyvinyl alcohol
HEX	Heat exchanger
SP	Specific power
SCP	Specific cooling power
COP	Coefficient of performance
SHTS	Sorption heat transformer systems
SCS	Sorption cooling systems
VCS	Vapor compression systems
VCR	Vapor compression refrigeration
HTF	Heat transfer fluid
SEM	Scanning electron microscope
CFC	Chlorofluorocarbon
Wt. %	Weight ratio in percentage

Executive Summary

Motivation

The global cooling energy demand is projected to triple by 2050, which takes account of the likely effect of current policies and targets, with nearly 70% of the increase coming from the residential sector [1]. Meanwhile, countries accounting for more than 60% of global energy-related carbon emissions aim to bring their emissions down to net zero by 2050 or soon after [2]. As more than 80% of residential building energy consumption is used for heating and cooling purposes, there is a rising interest in efficient and sustainable heating, cooling, and thermal storage (heat transformer) systems that do not add more CO_2 to the environment [3]. One promising solution is heat-driven sorption technology. Sorption systems that use benign environmentally friendly refrigerants such as water, have no noise or vibration problems, and can generate cooling power from low-grade industrial waste heat or renewable thermal energy sources with temperatures below 90°C, such as solar or geothermal heat [4].

High porosity sorbent materials - typically in the form of packed beds or consolidated composite coatings in sorption systems - often have low thermal conductivity and thermal diffusivity which impedes their heat transfer adversely affecting the overall performance. Low heat and mass transfer in sorbents result in low specific power (SP) which is one of the major limitations facing the commercialization of sorption heat transformer systems. Therefore, thermal conductivity of the consolidated sorbent layer is a fundamental property of the composite that can strongly affect the dynamic performance of sorption systems.

Several methods to enhance the heat transfer in sorption composites have been investigated. One common approach has been the addition of thermally-conductive additives, which, when combined with sorbent and binder, form higher conductivity paths to increase the overall thermal performance [5][6][7][8][9][10]. The main challenge with this method is that the thermal conductivity of composites can vary not only with composition, specifically the shape and volume percentage of the additive, but also with the preparation conditions if they affect the overall density.

During the sorption and desorption processes, the variation in sorbate (water) content can significantly affect the thermal conductivity and thermal diffusivity of the consolidated sorption composites. For instance, Tanashev et al. showed that the thermal conductivity

of $CaCl_2$/silica gel KSK increased ~ 285% from 0.13 to 0.5 $W \cdot m^{-1} \cdot K^{-1}$, as the absorbed water content increased from 0.1 to 0.8 $g \cdot g^{-1}$ [11]. Although, there is clear evidence of the dependence of thermal conductivity (k) on sorbate uptake in the majority of available models of sorption systems, it is assumed to be a constant value [12][13][14][15]. Furthermore, there is no mechanistic model that can predict the thermal conductivity/diffusivity of such composites, as a function of pertinent morphological and operating conditions, during the de/sorption process.

This study aims to address the above-mentioned challenges and presents a new analytical model that provides a reliable and easy-to-use compact relationship that can be utilized as a useful tool to enhance the heat transfer and overall performance of sorption systems.

Objectives

The main objective of this research project is to establish a systematic method to investigate and understand the effect of key morphological and operational parameters on the effective thermal conductivity of sorbent composites and how those would change the performance of sorption process in various applications. This study includes analytical modeling, sample preparation, and thermal properties measurement/characterization that can be used by thermal engineers to improve the thermal performance of sorption energy systems.

Research methodology

To attain the objective of this study, a systematic approach is utilized. The milestones of this methodology are highlighted in the following:

- Identify the key morphological parameters, material properties, and operating conditions that dominate the heat and mass transfer performance of sorbent composites;

- Develop a new analytical quasi- steady-state model to predict the effective thermal conductivity and thermal diffusivity of sorbent composites. The proposed closed-form solution, includes all salient morphological parameters, material properties, and operating conditions;

- Conduct a comprehensive parametric study to investigate the impact of water uptake, porosity, pore size, thermally-conductive additive type, and additive content on the effective thermal conductivity of the consolidated sorbent composite;

- Prepare a number of consolidated sorbent composites, including highly-conductive additive materials;

- Characterize the material and measure the thermal conductivity, thermal diffusivity, and specific heat capacity of sorbent composites in several operating conditions; and

- Design an experimental testbed to study the water uptake impact on the thermal conductivity and thermal diffusivity of the sorbent composites.

Research Roadmap and Contributions

The research roadmap for accomplishing the objectives is proposed in the following:

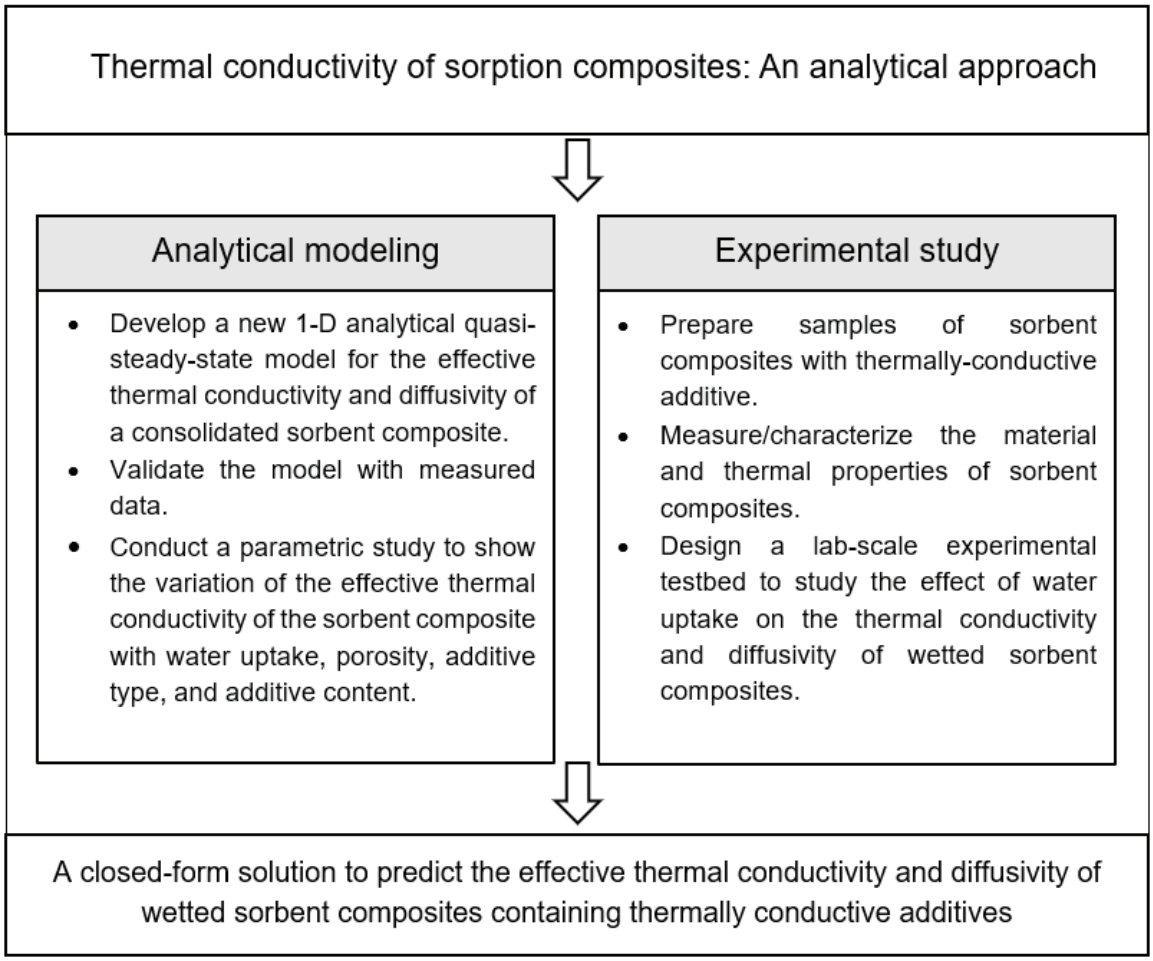

The major contributions of this research project are listed below:

1. A new 1-D analytical quasi- steady-state model was developed that considers key morphological parameters, material properties, and operating conditions, including thermal conductivity, specific heat capacity, and density of the sorbent and additive materials, host matrix pore size distribution, porosity, thermally-conductive additive type, additive content, water uptake, and temperature to predict the effective thermal conductivity and diffusivity of the consolidated

sorbent composite under the normal operating conditions of an adsorption or absorption system;

2. A comprehensive parametric study was carried out and the effects of water uptake, porosity, additive type, and additive content on the effective thermal conductivity of the consolidated sorbent composite were evaluated;

3. A number of new tailored composite sorbent materials with significantly improved thermal properties were prepared and characterized using graphite flakes and expanded natural graphite as thermally-conductive additives;

4. Thermal properties, namely, thermal conductivity, thermal diffusivity, and specific heat capacity of the sorbent composites were measured using a transient plane source method [16], over a range of water uptake levels;

5. Thermal conductivity of composite sorbent was significantly enhanced; up to 572% increase was observed from 0.11 to 0.74 $W \cdot m^{-1} \cdot K^{-1}$, by adding 5 wt.% of expanded natural graphite for a SG, $CaCl_2$, PVA sorption composite when tested at 2% RH and 25°C; and

6. Thermal diffusivity of composite sorbent was noticeably improved; up to 650% increase was observed from 0.12 to 0.90 $mm^2 \cdot s^{-1}$, by adding 15 wt.% of graphite flakes for a SG, $CaCl_2$, PVA sorption composite when tested at 2% RH and 25°C.

Chapter 1.

Introduction and literature review

Global primary energy consumption has increased more than 130% in the last 45 years due to massive increases in population, energy demand, and industrial activities. The building sector is responsible for 32% of global final energy demand (24% residential and 8% commercial), and for 30% of energy-related CO_2 emissions [17][18]. Heating and cooling systems account for more than 60% of residential and nearly 50% of commercial building energy consumption, shown in Figure 1.1. Vapor-compression systems (VCS) are the most cost-effective heating and cooling technologies currently available and form 99% of space-cooling energy consumption in the US [19]. They are, however, powered by electricity, which is still mostly derived from non-renewable sources, including coal and oil. In addition to the energy sources of VCS, they use chlorofluorocarbon (CFC) refrigerants, which contribute to global warming due to their greenhouse gas (GHG) emission effects.

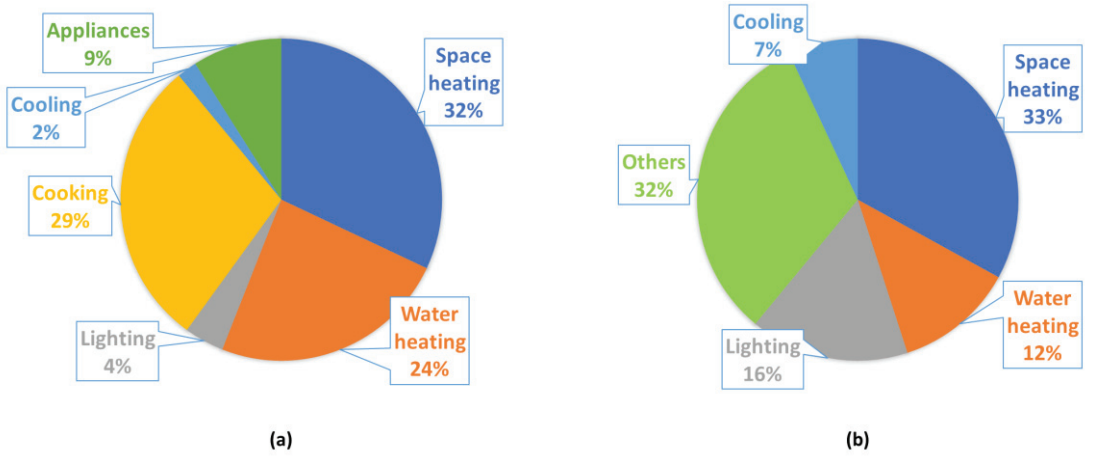

Figure 1.1. (a) Residential buildings global final energy consumption; and (b) Commercial buildings global final energy consumption [17].

Countries accounting for more than 60% of global energy-related carbon emissions, including US and Canada, aim to bring their emissions down to net zero by 2050 or soon after [2]. This brings attention to efficient and sustainable heat transformer (heating, cooling, and thermal storage) systems that do not add more CO_2 to the environment [3]. Abundant low-grade thermal energy sources in the transportation,

industrial, and building sectors, including waste heat available in the form of steam, hot water, furnaces, boilers, engine exhaust, drier, air compressors, and solar energy, made heat-driven sorption technology one of the most promising solutions [20]. Sorption systems that use environmentally friendly refrigerants like water, have no noise or vibration issues, and can produce cooling power from low-grade industrial waste heat or low-temperature renewable thermal energy sources like solar or geothermal heat [4].

It can be seen from the global heat distribution illustrated in Figure 1.2, that more than 50% of the global primary energy is wasted in the form of heat [21]. Furthermore, it is shown in Figure 1.2 that comparing to high-grade (T>300°C) and medium-grade (100°C<T<300°C) waste heat, the low-grade (T<100°C) comprises 63% of the global waste heat.

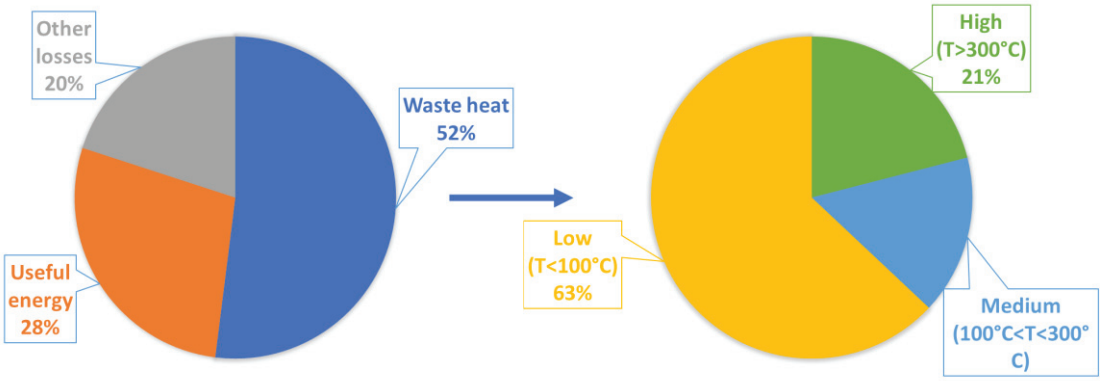

Figure 1.2. Global waste heat distribution with their temperature levels in 2016 [21].

Sorption systems can implement the low-grade waste heat to the following applications:

i. Generate cooling for air-conditioning and refrigeration;

ii. Store thermal energy;

iii. Upgrade the heat to a higher temperature level;

iv. Heat pumping;

v. Dehumidification; and

vi. Gas separation.

However, the main limitations of sorption systems, include high cost, low specific power, and poor heat exchanger heat and mass transfer that is caused by low sorbent thermal conductivity and thermal diffusivity. The present study focuses on the thermal conductivity and diffusivity of sorbent composites and presents a new analytical model that provides a reliable and easy-to-use compact relationship that can be utilized as a useful tool to enhance the heat transfer and overall performance of sorption systems.

1.1. Sorption heat transformer systems (SHTS)

1.1.1. Sorption phenomena

The general term sorption is used when both adsorption and absorption occur simultaneously. Sorption is a surface phenomenon that occurs at the interface of two phases and happens when cohesive forces, such as Van der Waals forces and hydrogen bonding function between the molecules of all substances, regardless of their aggregation state. Surface forces or unbalanced forces at the phase boundary cause changes in the concentration of molecules at the solid/fluid interface. The solid and the fluid adsorbed on the solid surface are referred to as sorbent and sorbate, respectively [22].

Sorption may occur as a result of a physical process known as physical sorption, or physisorption, which is caused by Van der Waals forces, or a chemical process called chemical sorption, or chemisorption, which is caused by valency forces. Physisorption is largely controlled by surface properties, such as surface area, micro- and macro-pores, and the size of the grains [23]. Chemical forces between the pairs are much stronger than physical forces [24]. Regardless of the form of sorption, the evolution of heat of adsorption exists in both cases. The desorption process, which typically involves the application of heat, will restore sorbent substances to their original state, except in certain cases where chemisorption processes are irreversible [22].

1.1.2. Thermodynamic of sorption cycle

In a vapor compression refrigeration (VCR) system, the low-pressure, and low-temperature refrigerant reaches the compressor as a saturated vapour and is compressed to raise its pressure and temperature. The superheated vapour refrigerant is then condensed in the condenser, releasing heat into the atmosphere. The saturated liquid

refrigerant then passes through an expansion valve or a capillary tube to reduce its pressure and prepare for the low-temperature evaporation process. Finally, in the evaporator, the refrigerant, which is a mixture of liquid and vapour phases at this stage, is evaporated, providing the cooling effect. Figure 1.3 shows the schematic diagram of a VCR system.

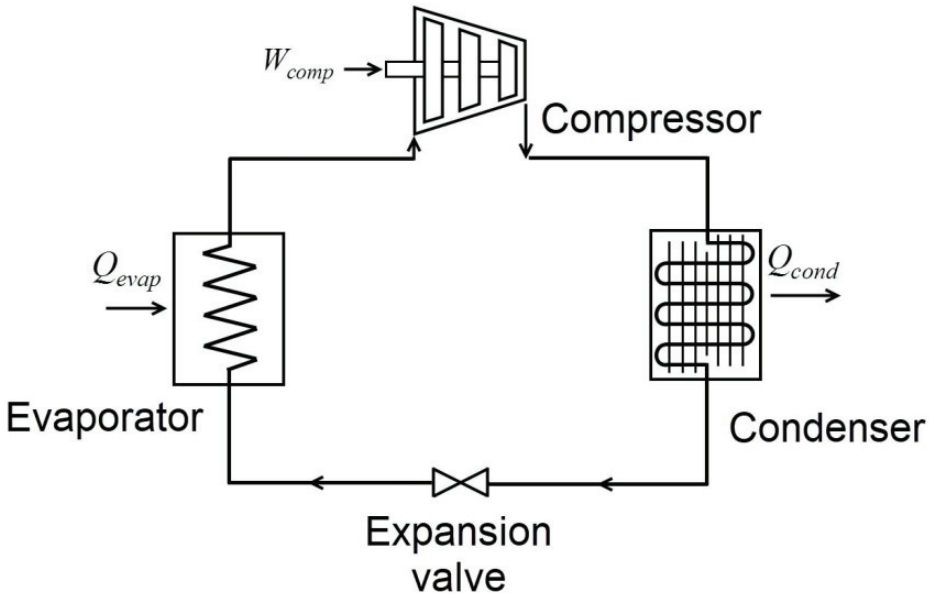

Figure 1.3. A schematic diagram of VCR systems [25].

Sorption heat transformer systems on the other hand, function based on two main steps: Heating–desorption–condensation, and cooling–adsorption–evaporation. In sorption heat transformer systems (SHTS), as shown in Figure 1.4, the compressor in VCR is replaced with sorber bed heat and mass exchangers consisting of: (i) a heat exchanger; (ii) sorbent material in the form of grains, pallets, or coating; and (iii) heat transfer fluid (HTF). Ad/absorption and desorption by sorbent material happens when the sorbate is cooled and connected to the evaporator, and when it is heated and connected to the condenser at a higher pressure. The heating and cooling process is done by HTF through a heat exchanger. Consequently, heat, rather than the compressor in VCR systems, provides the increase in pressure to compress the refrigerant which is the driving force in the refrigeration cycles. Therefore, instead of mechanical work from engines or electrical energy in VCR, waste heat and solar energy can be used to power the refrigeration cycle.

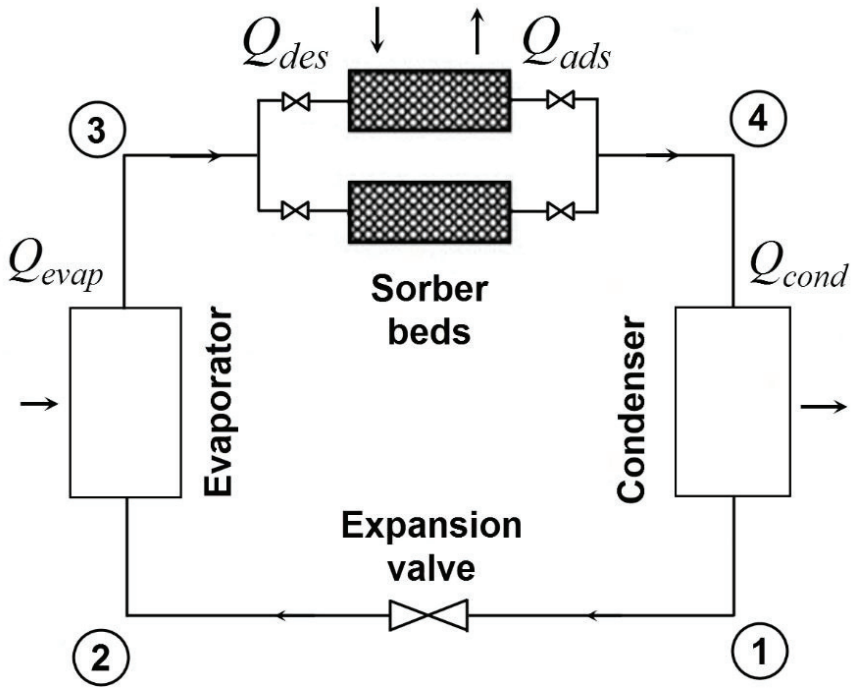

Figure 1.4. A schematic diagram of sorption heat transformer systems [25].

The thermodynamic cycle of a sorption heat transformer system shown in Figure 1.5 consists of four main steps: (i) Isosteric cooling: Both valves between the sorber bed and evaporator and condenser are shut and the sorbent loses its heat during an isosteric cooling process (Step 1'-2'). At the same time, the sorbate inside the condenser passes through an expansion valve to reduce its pressure, Step 1-2; (ii) Isobaric adsorption: During Step 2-3, the valve to the evaporator is opened. The sorbate enters the evaporator, absorbs heat from the environment and evaporates. At the same time, the valve between the sorber bed and evaporator is open and the vapor sorbate is adsorbed at a constant pressure and releases its heat, Step 2-3; (iii) Isosteric heating: During Step 3-4, the sorbent material absorbs heat from an external heat source through an isosteric process. Both valves are closed at this step to prepare the sorber bed for the desorption process. The heating process at a constant uptake is continued until the sorber bed pressure equals the condenser pressure; (iv) Isobaric desorption: Finally, the entrance valve to the condenser is opened. In Step 4-1, the external heat source continuously heats the sorber bed because of the endothermic desorption and the sorbate leaves the sorber bed. In Step 4-1, the sorbate is condensed in the condenser.

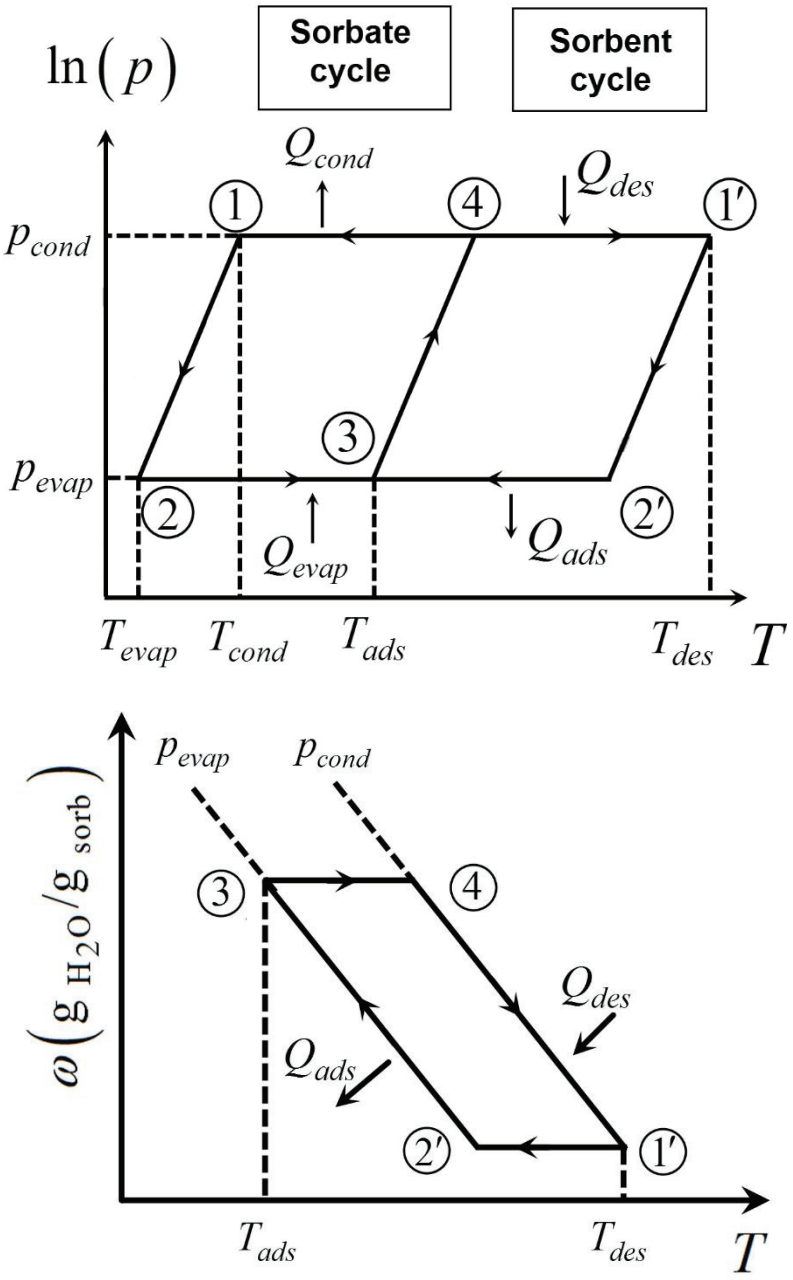

Figure 1.5. The thermodynamic cycle of sorption heat transformer systems.

1.2. Heat and mass transfer improvement in sorption systems

1.2.1. Thermal conductivity and diffusivity of sorbent composites

Commercialization of sorption heating and cooling systems is limited by fundamental challenges, including low specific cooling power (SCP) and low coefficient of performance (COP) because of poor heat transfer between the sorber bed heat exchanger (HEX) and the sorbent material [9].

During the sorption and desorption cycles, sorber beds must be cooled and heated, respectively. As a result, the sorbent thermal diffusivity is critical in the efficiency of sorption cooling systems (SCS) due to their oscillatory thermal nature. One of the key limiting factors in heat transfer between the sorbent and the heat transfer fluid (HTF) through the heat exchanger is sorbent thermal diffusivity. Thus, increasing the thermal diffusivity of sorbent composites can improve the overall efficiency of sorption heat and mass exchangers [25].

However, it is important to note that many approaches, including adding thermally-conductive additives to enhance the heat transfer in sorption composites not only cause an improvement in thermal conductivity and diffusivity but also, at the same time, decrease the active sorption material fraction affecting the total sorption capacity. Hence, there is a trade-off between the heat transfer and sorption capacity which should be considered when improving the sorption system performance.

1.2.2. Heat and mass transfer improvement in sorption systems using thermally-conductive additives

Several methods to enhance the heat transfer in sorption composites have been investigated. One common approach has been the addition of thermally-conductive additives, which, when combined with sorbent and binder, form higher conductivity paths to increase the overall thermal performance [5][6][7][8][9][10]. The main challenge in this method is that the thermal conductivity of composites can vary not only with composition, specifically the shape and volume percentage of the additive, but also with the preparation conditions if they effect the overall density.

A summary of existing studies on adding thermally-conductive additives to enhance the heat and mass transfer of sorption systems is presented in Table 1.1. Demir et al. [26] investigated the effect of metal piece additives, including copper, brass, aluminum, and stainless steel on the effective thermal conductivity and diffusivity of an unconsolidated silica gel-based sorbent composite. They used 1.0-2.8 mm and 2.8-4.75 mm additive sizes and developed a dimensionless heat conduction equation to predict the effective thermal conductivity and diffusivity of the mixed bed. They observed a 157% increase in thermal conductivity and a 242% increase in thermal diffusivity of a pure silica gel bed with the addition of 15 wt.% of 1.0 to 2.8 mm-sized aluminum particles. Askalany et al. [8] studied the impact of adding 10 to 30 wt.% of metallic additives, including iron, copper, and aluminum on the thermal conductivity of granular activated carbon (1-2 mm). They reported that thermal conductivity was increased by increasing the metallic additives concentration. They also noticed that the addition of 30 wt.% of aluminum additives increased the specific cooling power of their adsorption cooling system by 100%. Nevertheless, metallic additives are not appropriate for corrosive sorbent materials such as salt in porous matrix composites as they cause outgassing and create non-condensable gases that kill sorption kinetics. Graphite-based additives like graphite flakes (GF) or expanded natural graphite (ENG) on the other hand, are better candidates when a corrosive sorbent is used. Additionally, graphite has a higher intrinsic thermal conductivity, a lower molecular weight, and excellent stability at high working temperatures than most metals [27]. Therefore, it is a suitable additive to improve the thermal conductivity and thermal diffusivity of sorption composites which consequently, enhances the SCP of the sorption system.

High thermal conductivity of graphite, along with the other above-mentioned benefits, made it the most studied additive for developing sorbent composite with the aim of improving thermal conductivity [28]. Mauran et al. [29], for example, reported the thermal conductivity of their $CaCl_2$-ENG sorbent composites to be 10 to 40 $W \cdot m^{-1} \cdot K^{-1}$. Wang et al. [6] measured the thermal conductivity for three types of sorbents namely, simple unconsolidated sorbent composite, consolidated sorbent composite with expanded graphite as additive, and pure $CaCl_2$ powder using the hot wire method. They reported that the thermal conductivity of the $CaCl_2$-expanded graphite consolidated sorbent composite to be in the range of 7.05 to 9.2 $W \cdot m^{-1} \cdot K^{-1}$ depending on the mass fraction of expanded graphite. Fayazmanesh et al. [10] studied the effect of adding graphite flakes

as a thermally-conductive additive to a sorbent composite made of $CaCl_2$ in a silica gel matrix. The thermal conductivity of a set of sorbent composites made of silica gel B60 (B represents the particle size range of 200 to 500 μm, and 60 represents the average particle size reported by the supplier as 60 Å), $CaCl_2$, and PVP40 with 0–15 wt. % of graphite flakes were measured at 2 and 20 RH% using a transient plane source (TPS) method. Their result indicates that the addition of 20 wt.% of graphite flakes increased the thermal conductivity of the sorbent composite from 0.57 to 0.78 $W \cdot m^{-1} \cdot K^{-1}$. Eun et al. [5] investigated the effect of adding expanded graphite to sorbent composites made of silica gel. They also studied the effect of porosity on the sorbent thermal conductivity. Their results show the thermal conductivity of sorbent composites increased from 0.17 $W \cdot m^{-1} \cdot K^{-1}$ to a thermal conductivity range of 10 to 20 $W \cdot m^{-1} \cdot K^{-1}$ depending on the expanded graphite mass ratio in the composite. Zheng et al. [7] studied the effect of adding expanded natural graphite treated with sulfuric acid (ENG-TSA) to a silica gel sorbent composite to improve the thermal conductivity and adsorption performance of the composite. Their evaluation on non-equilibrium adsorption performance and equilibrium adsorption performance showed enhancement of both heat and mass transfer, respectively. They also reported that by adding ENG to the silica gel composite, they measured the maximum thermal conductivity of 19.1 $W \cdot m^{-1} \cdot K^{-1}$, which is 270 times higher than their pure silica gel composite.

Table 1.1. A summary of existing studies on the effect of thermally-conductive additives on heat and mass transfer of sorbent composites.

Ref. No.	Year	Sorbent material	Thermally-conductive additive	Increase in thermal conductivity ($W \cdot m^{-1} \cdot K^{-1}$)	Impact on uptake
[29]	1993	$CaCl_2$ and ENG	Expanded natural graphite	Up to 30	Not reported
[30]	1994	Zeolite	Expanded graphite	0.09 to 10	Not reported
[31]	1997	Zeolite 4A	Graphite (40 wt.%)	0.1 to 0.35	Equilibrium uptake decreased from 0.23 to 0.13 ($g_{water}/g_{sorbent}$)
[5]	2000	Silica gel	Expanded graphite	Up to 19	Transient uptake increased
[6]	2006	$CaCl_2$	Expanded graphite	Up to 9.2	Not reported
[26]	2010	Silica gel	Copper, brass, aluminum, and stainless steel	157% increase	Not reported
[7]	2014	Silica gel	Expanded natural graphite	Up to 20	Transient uptake increased
[8]	2017	Granular activated carbon	Iron, copper, and aluminum (10 to 30 wt.%)	Increased with additive concentration	Not reported
[10]	2017	$CaCl_2$ and silica gel	Graphite flakes (0 to 20 wt.%)	0.57 to 0.78	Equilibrium uptake decreased

Chapter 2.

Analytical modeling

2.1. Literature review

A summary of published investigations of water uptake (ω) impact on the effective thermal conductivity of wetted porous medium and their studied parameters is presented in Table 2.1. The first study of the effect of water sorption on the thermal conductivity of a $SiO_2/CaCl_2$ system was carried out in [32] using a hot wire method [33]. They reported that thermal conductivity increased from 0.33 to 0.53 $W \cdot m^{-1} \cdot K^{-1}$ when the water uptake changed from 0.35 to 0.75 $g \cdot g^{-1}$. Freni et al. [34] measured the thermal conductivity of two composite sorbents made of silica gel with $CaCl_2$, or LiBr as the salt, using a hot wire method under various conditions of vapor pressure (P_{wv}), temperature (T), and water uptake. They observed a 0.10 and 0.15 $W \cdot m^{-1} \cdot K^{-1}$ increase, respectively, in the thermal conductivity of their composites if the measurement ranges were chosen according to the operating conditions of a typical sorption cooling cycle (10 mbar < P_{wv} < 70 mbar, 40°C < T < 130°C).

Buonanno and Carotenuto [35] developed a model to predict a porous medium's effective thermal conductivity. Steady-state heat conduction in a two-phase system was studied using a volume averaging technique. Particle shape, roughness, and solid conductivity were also investigated. McGaughey and Kaviany [36] presented a molecular dynamic simulation-based analysis for thermal conductivity of a porous structure. The applied molecular dynamic simulation was rather sophisticated to be utilized in adsorption heat pump system simulations. Lu et al. [37] experimentally studied the effects of porosity, particle size, and natural convection on the effective thermal conductivity of a copper foam-air and copper foam-water system. A linear correlation to describe the contribution of fluid was proposed as a function of porosity and pore size. Dawoud et al. [38] developed a theoretical model for predicting the effective thermal conductivity of wetted zeolite. To validate their model, the effective thermal conductivity of 4A zeolite-water was measured by a transient hot wire method under various conditions of vapor pressure, temperature, and water loading representing a typical adsorption cooling cycle. However, various

parameters were estimated by fitting the experimental data which limits the application of the model to a specific composite.

Aristov et al. [39], measured the dependence of the thermal conductivity of the two-component sorbent $SiO_2/CaCl_2$ on the sorbed water uptake. They also measured the thermal conductivity of sorbents made of mesoporous silica gel and alumina with an impregnated salt ($CaCl_2$, $MgCl_2$, and $LiBr_2$) [11]. For the three silica-based sorbents, similar dependencies of effective thermal conductivity as a function of uptake, $k(\omega)$, were found as: i) a smooth rise at $\omega < \omega^* = 0.4 – 0.55$, where ω^* is the uptake threshold (i.e., in this case, when the mesopores of silica gel are completely filled with the salt solution); and ii) a sharp increase within the narrow uptake range near the threshold uptake ω^*. The transition occurs at the same fraction of the pore volume occupied by the salt solution regardless of the salt confined. Their obtained results were described by a heat transfer model in a porous wetted medium developed by Luikov [40] and modified by Bjurstrm [41]. Fayazmanesh et al. [10] studied the effect of water uptake on the effective thermal conductivity of the sorbent composite $SiO_2/CaCl_2$ and graphite flake as a thermally-conductive additive. The thermal conductivity of a set of sorbent composites made of silica gel B60, $CaCl_2$, and PVP40 with 0–15 wt. % of graphite flakes were tested at 2 and 20 RH%. The increase in the absorbed water content from 0.06 to 0.19 $g \cdot g^{-1}$ was shown to increase the thermal conductivity of the sample from 0.3 to 0.48 $W \cdot m^{-1} \cdot K^{-1}$.

Table 2.1. A summary of the existing studies on the effect of water uptake on the effective thermal conductivity of sorption composites.

Ref. No.	Sorbent/host matrix	Salt	Approach	Characteristics of the parametric study
[11], [39]	Silica gel Alumina	$CaCl_2$ LiBr $MgCl_2$	Experimental	Water uptake Salt material Host matrix material
[38]	Zeolite 4A	—	Experimental Theoretical model	Water uptake Temperature
[34]	Silica gel	$CaCl_2$ LiBr	Experimental	Water uptake Salt material Temperature Vapor pressure
[35]	—	—	Volume averaging model	Particle shape Roughness Solid conductivity
[36]	Silica Zeolite-A	—	Molecular dynamic simulation	Water uptake
[41]	Silica gel	—	Analytical model Experimental	Water uptake Porosity Temperature Total gas pressure
[10]	Silica gel	$CaCl_2$	Experimental	Water uptake Additive particle (Graphite flakes)
[37]	Copper foam	—	Experimental	Air and water uptake Porosity Natural convection

To the best of the authors' knowledge, no prior study investigated the effects of all salient parameters, including water uptake, porosity, and thermally-conductive additives simultaneously on the effective thermal conductivity of sorption composites. The absence of a mechanistic closed-form solution (meaning that it can be expressed analytically in terms of a finite number of certain functions) for the effective thermal conductivity of sorbent composites is noticeable.

This study aims to fill this knowledge gap by developing a new 1-D quasi- steady-state analytical model for the effective thermal conductivity and diffusivity of a consolidated salt-in-matrix sorption composite. This methodology can be applied to other sorts of sorption composites as well. The model considers the key morphological and operational parameters, including thermal conductivity, porosity, pore size distribution, and density of the host matrix, along with the thermal conductivity, density, aspect ratio (the ratio of the diameter to the thickness of an additive particle), and size of the thermally-conductive additive particles to determine the water uptake impact on the effective thermal conductivity of the composite during a sorption working cycle.

2.2. Model development

2.2.1. Thermal conductivity of the effective medium

In this study, an analytical model for the effective thermal conductivity of the sorbent composite is developed based on a unit cell approach, where the thermal conductivity calculation is made for an elementary cell, shown in Figure 2.3(b), as a representative of the entire effective medium. Therefore, the thermal conductivity of the composite is equal to that of the unit cell. It is assumed that the heat conduction in the unit cell is one-dimensional, which leads to the isothermal top and bottom surfaces, while the lateral walls are adiabatic due to symmetry [42]. It is also assumed that the natural convection in the small pores between the sorbents can be neglected [43], and radiation is also negligible at low temperatures (below 600°C [44]). Therefore, heat transfer occurs via conduction through the solid host matrix and conduction through the interstitial gas.

As shown in the scanning electron microscope (SEM) image of Figure 2.1, and schematically presented in Figure 2.2(a), the porous sorbent composite is represented as a periodical structure with a skeleton so that the unit cell with a simple geometry may be segregated. Moreover, due to symmetry, the unit cell here is 1/16 of the periodical cubic structure shown in Figure 2.2(b). Following the methodology introduced by Luikov [40] and modified by Bjurstrom [41], some modifications have been made to the unit cell to better represent the morphology of the sorbent composite. Figure 2.3(a) shows the unit cell right-

view, including the main geometrical parameters. The size of the unit cell depends on the average pore size diameter of the host matrix (d_p).

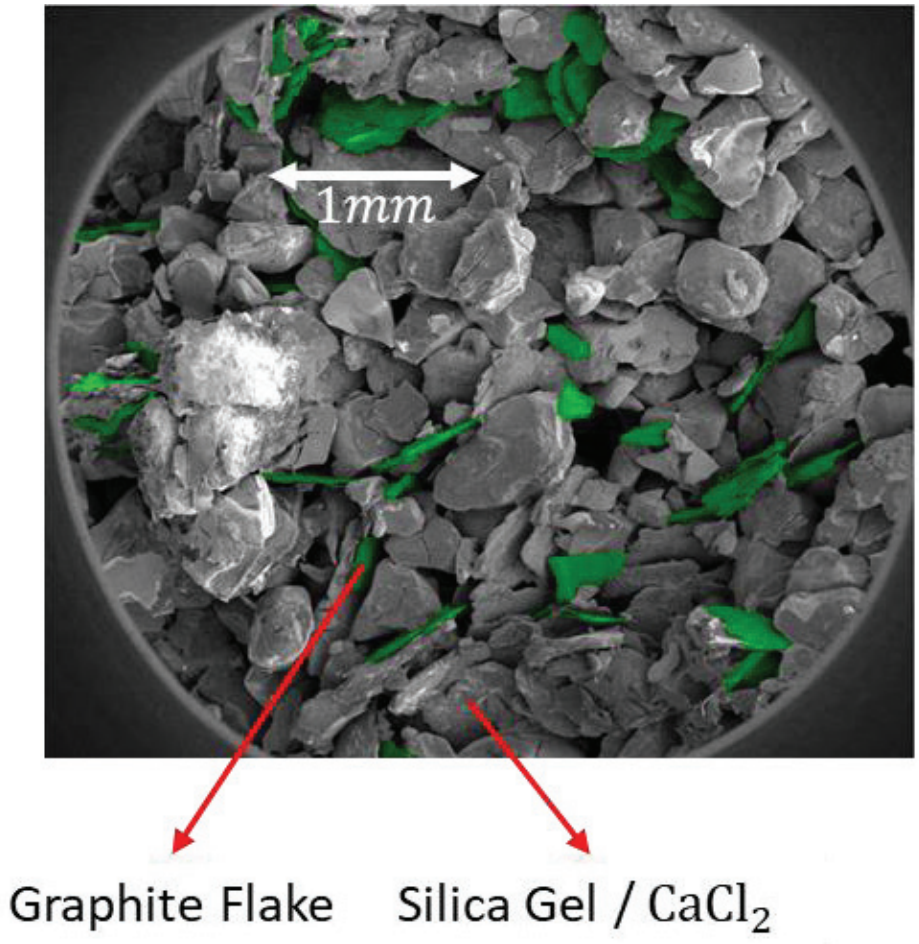

Figure 2.1. An SEM image of a composite sorbent made with SG-$CaCl_2$-PVA and 20 wt.% of graphite flakes (colored in green) [9].

The model is developed for sorbents consisting of silica gel, salt, binder, and conductive additive particles used for both adsorption and absorption processes. Silica gel and $CaCl_2$ are chosen as the baseline sorbent pair due to their wide range of operating conditions for sorption, and their low cost, which is a major matter when it comes to commercialization of sorption systems.

The assumptions used in the development of the present model are:

- Thermodynamic equilibrium of the sorbent composite at each partial pressure. Therefore, the uptake of the sorbent particles corresponds to the equilibrium water

uptake at a steady-state temperature and relative humidity (or pressure ratio, P/P_{sat}, for the closed adsorption systems);

- The binder effect is neglected due to its low concentration;
- The contact between graphite additive particles and the sorption material is perfect, i.e., no thermal contact resistance is considered;
- The sorption material and graphite additive particles have constant anisotropic properties, listed in Table 2.2;
- Based on a previous study performed in our lab [45], the angle of additive particles (θ) is assumed to be 45°. This assumption can also be justified by considering the fact that the additive particles distribution in the composite is random (Gaussian distribution), thus, the angles could vary from 0 to 90 degrees;
- Uniform pore size diameter is considered; the average measured pore size is used; and
- The absorbed water is considered as a distributed film with a uniform thickness of t_w around the solid skeleton of the host matrix.

Table 2.2. Material and geometrical properties of the sorption composites.

Silica Gel		**Graphite Flakes**				**Expanded Natural Graphite**		
True density ($g \cdot cm^{-3}$) [11]	k_{Silica} ($W \cdot m^{-1} \cdot K^{-1}$) [11]	Bulk density ($g \cdot cm^{-3}$) [45]	$k_{Graphite}$ ($W \cdot m^{-1} \cdot K^{-1}$) [46]	r_{GF} (μm) [45]	t_{GF} (μm) [45]	Bulk density ($g \cdot cm^{-3}$) [47]	r_{ENG} (μm) [47]	t_{ENG} (μm)
2.4	1.35	0.64	8	544	4.3	0.04	40	81

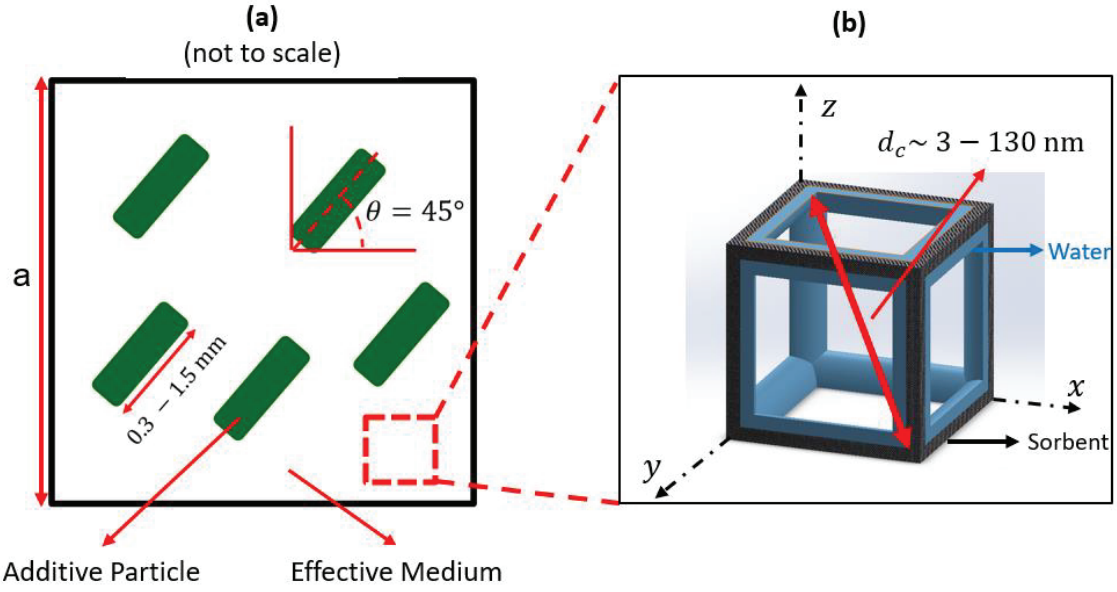

Figure 2.2. (a) The effective medium illustration (not-to-scale), thermally-conductive particle angle (θ) is assumed to be 45 degrees, based on [20]; and (b) The silica gel pore unit cell model proposed in this study.

Using the above assumptions, a thermal resistance network is developed to represent the heat conduction in the unit cell shown in Figure 2.3(b). The thermal resistance of network consists of four thermal paths illustrated in Figure 2.4(a): i) bulk thermal resistance of the solid silica, $R_{S,\frac{L}{2}}$; ii) resistance of the thermal path consisting of solid silica and absorbed water layers, $R_{sw,r_s}, R_{w,\frac{l_S}{2}}$; iii) resistance of the thermal path consisting of solid silica, interstitial gas (water vapor), and absorbed water layers, $R_{swg,r_w}, R_{g,\frac{l_W}{2}}$; and iv) resistance of interstitial gas in the mesopores, and intergranular pores of the sorbent composite, $R_{g,\frac{L}{2}}$.

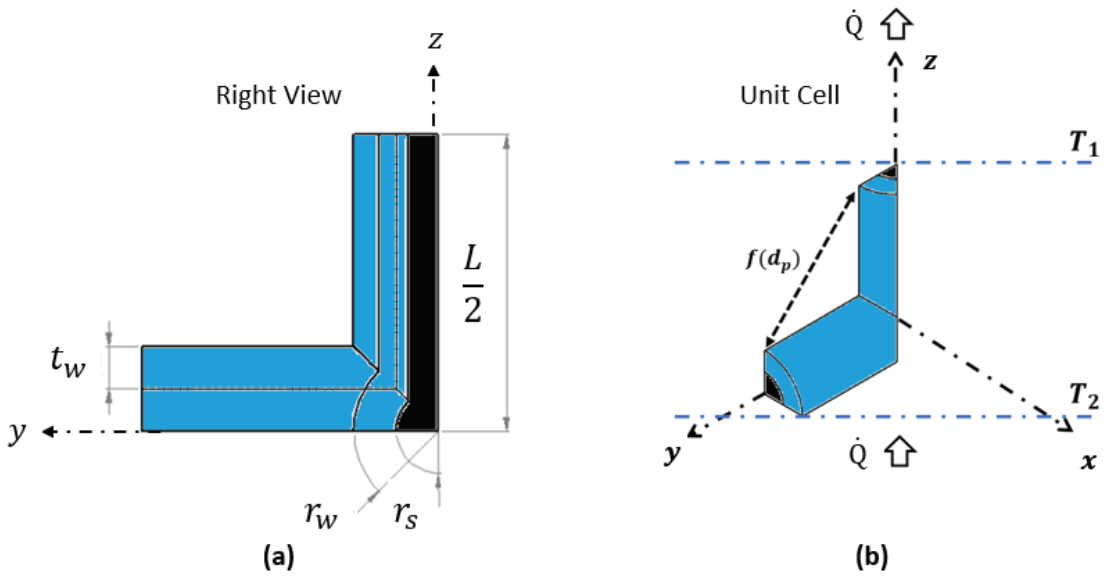

Figure 2.3. **(a) The right-view schematic of the unit cell; and (b) A schematic illustration of the unit cell. The unit cell here is 1/16 of the periodical cubic structure shown in Figure 2.2(b).**

The thermal resistance for each path is calculated based on the average pore size diameter, measured thermal conductivity, silica gel true density (i.e., the quotient of mass over the volume of a sample, without considering pores in the material (true volume)), and water density. The resistance of interstitial gas in the mesopores is calculated using the same method developed by Bahrami et al. [48], [49].

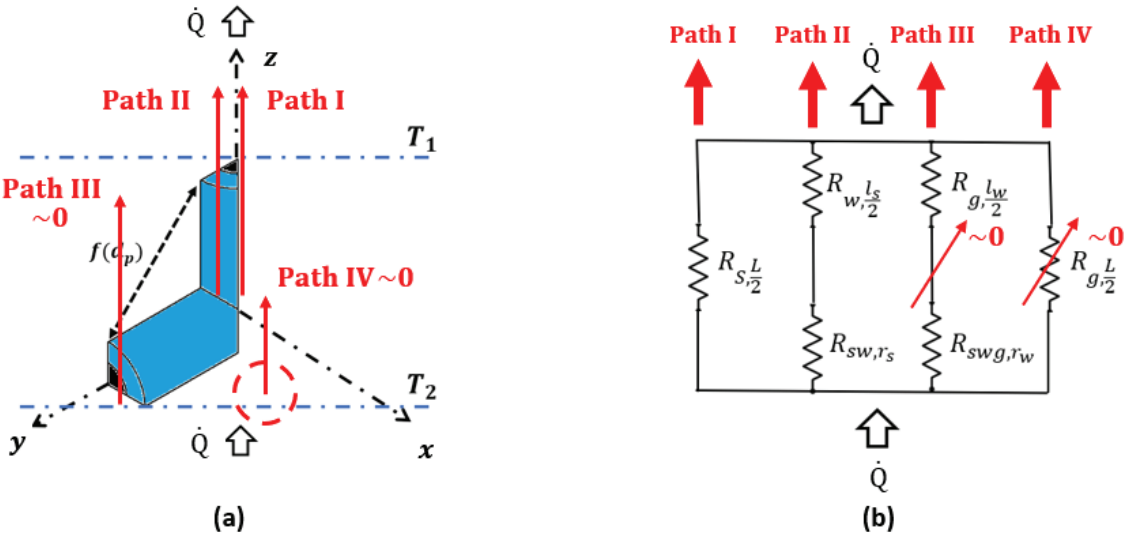

Figure 2.4. **(a) An illustation of thermal paths in the unit cell; and (b) The thermal resistance network diagram of the unit cell with corresponding thermal paths.**

The first index of the resistances stands for the medium through which heat is flowing, and the second index stands for the length of the path of heat through this medium.

To calculate the thermal resistances, First, three additional parameters defined as:

$$l_s = L - 2r_s \tag{1}$$

$$l_w = L - 2r_w \tag{2}$$

$$r_w = r_s + t_w \tag{3}$$

In thermal path (i), for conduction through the solid silica, $R_{S,\frac{L}{2}}$ defined as:

$$R_{s,\frac{L}{2}} = \frac{L/2}{k_s.\left(\frac{\pi r_s^2}{8}\right)} \tag{4}$$

Next, in path (iv), for the conduction through the water vapor gas phase in pores, $R_{g,\frac{L}{2}}$ defined as:

$$R_{g,\frac{L}{2}} = \frac{L/2}{k_g.\, l_w^2/8} \tag{5}$$

Path (ii) consists of two series of thermal resistances. The first one, R_{sw,r_s}, represents the combined solid/liquid water phase, which is indicated with two parallel resistances labeled; R_s, and R_w, respectively. The corresponding thermal resistance diagram and schematic of path (ii) is shown in Figure 2.5. Defining the horizontal element *dy,* we have:

$$y = rcos\theta_s \tag{6}$$

$$dy = -rsin\theta_s d\theta_s \tag{7}$$

$$R_s = \int_y^0 \frac{dy}{k_s.(rsin\theta_s).\frac{l}{2}} \tag{8}$$

$$R_w = \int_y^0 \frac{dy}{k_w.(r - rsin\theta_s).\frac{l}{2}} \tag{9}$$

therefore, R_{sw,r_s} is calculated using the following:

$$\frac{1}{R_{sg,r}} = \frac{1}{R_s} + \frac{1}{R_g} \tag{10}$$

by integrating the *dy* element for (0, *y*), R_{sw,r_s} is calculated as:

$$R_{sw,r_s} = \frac{1}{t_w}\int_0^{\frac{\pi}{2}} \frac{sin\theta_s d\theta_s}{(k_s.sin\theta_s + k_w.(1 - sin\theta_s))} \tag{11}$$

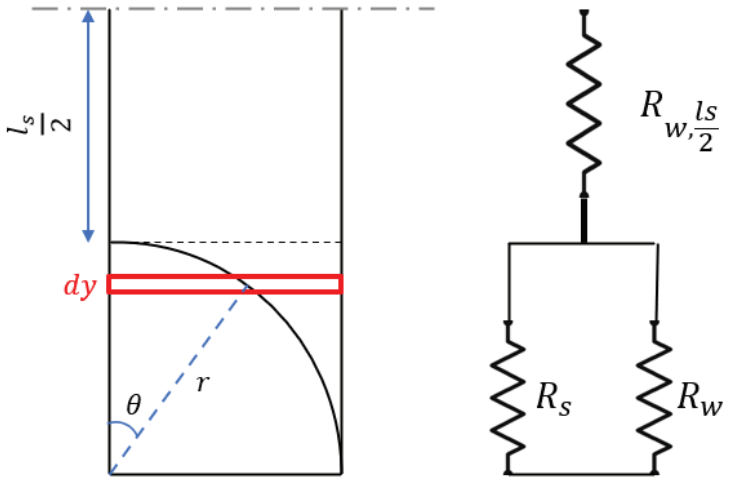

Figure 2.5. The side-view illustration and thermal resistance diagram of the combined solid/liquid phase in thermal path (ii) of Figure 2.4.

The second thermal resistance in this path, which represents the thermal resistance to conduction through the above liquid water phase, $R_{w,\frac{l_s}{2}}$, is written as:

$$R_{w,\frac{l_s}{2}} = \frac{l_s/2}{k_w.\frac{\pi}{8}.(r_w^2 - r_s^2)} \tag{12}$$

Thermal path (iii) is quite similar to path (ii) except that it consists of three solid, liquid, and gas phases each representing with a parallel resistance naming; $R_{s'}$, $R_{w'}$, and $R_{g'}$, respectively. The corresponding thermal resistance diagram and side-view

schematic for this path is shown in Figure 2.6. Following the same methodology used in path (ii), the horizontal element dy' is defined:

$$y' = r_s \cos(\theta_s) = r_w \cos(\theta_w) \tag{13}$$

$$dy' = -r_s sin\theta_s d\theta_s \tag{14}$$

The thermal resistances for each layer are written as:

$$R_{s'} = \int_y^0 \frac{dy'}{k_s.(rsin\theta).\frac{l_w}{2}} = \int_0^{\frac{\pi}{2}} \frac{r_s Sin\theta_s d\theta}{k_s r_s Sin\theta_s.\frac{l_w}{2}} = \frac{\pi}{k_s l_w} \tag{15}$$

$$R_{w'} = \int_y^0 \frac{dy'}{k_w r_w Sin\theta_w.\frac{l_w}{2}} \tag{16}$$

$$R_{g'} = \int_y^0 \frac{dy'}{k_g.(r_w - r_w sin\theta_w).\frac{l_w}{2}} \tag{17}$$

consequently, for conduction through the combined solid/liquid/gas, R_{swg,r_w} is calculated as:

$$R_{swg,r_w} = \left(\frac{1}{R_s} + \frac{1}{R_w} + \frac{1}{R_g}\right)^{-1} \tag{18}$$

integrating the dy' element for $(0, y')$ results in:

$$R_{swg,r_w} = \frac{k_s l_w}{\pi} + \left(\frac{2}{l_w}\int_0^{\frac{\pi}{2}} \frac{sin\theta_w d\theta_w}{(k_w.sin\theta_w + k_g.(1 - sin\theta_w))}\right)^{-1} \tag{19}$$

The other thermal resistance in path (iii), which represents the resistance to conduction through the pore area above the uptake layer, $R_{g,l_w/2}$, is calculated as:

$$R_{g,l_w/2} = \frac{l_w/2}{k_g.\frac{l_w}{2}.r_w} = \frac{4}{k_g.r_w} \tag{20}$$

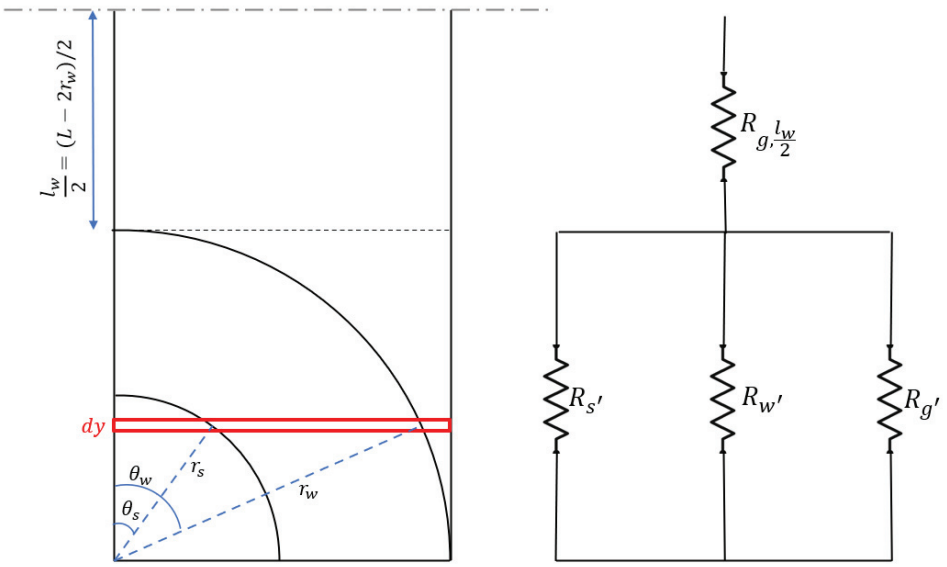

Figure 2.6. The side-view illustration and thermal resistance diagram of the combined solid/liquid/gas phase in thermal path (iii) of Figure 2.4.

Performing an order of magnitude analysis shown in Figure 2.7, the thermal resistances in paths (iii) and (iv) are an order of magnitude higher than the first two paths shown in Figure 2.4(b). This is due to the considerable difference in the thermal conductivity of water vapor as interstitial gas compared to that of solid silica and liquid water. Therefore, the simplified thermal resistance network shown in Figure 2.8 will include thermal paths (i) and (ii) only.

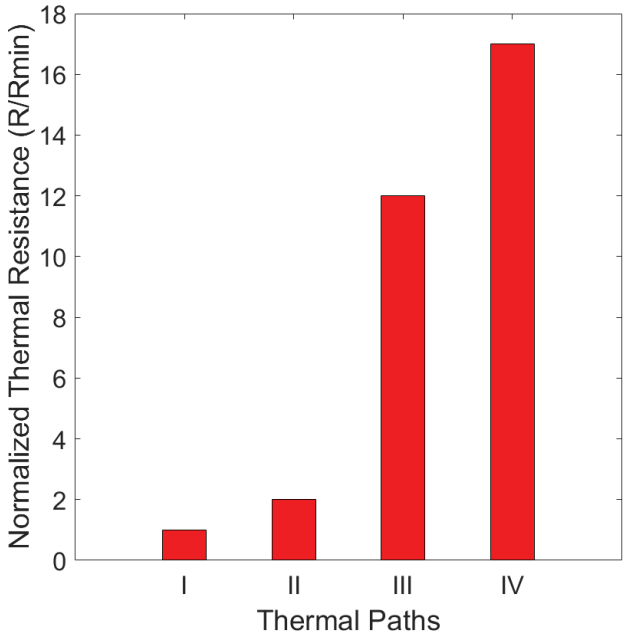

Figure 2.7. An order of magnitude analysis of thermal resistances in the thermal resistance network of the unit cell.

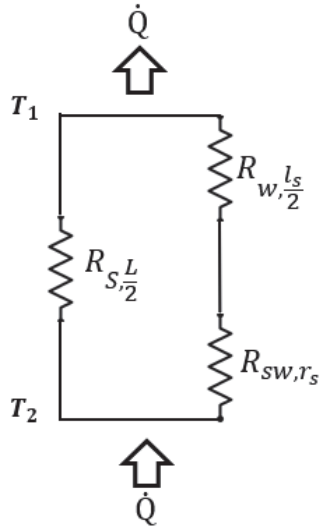

Figure 2.8. A simplified thermal resistance network diagram of the unit cell.

The thermal conductivity and density of the salt solution are calculated based on the mixing rule of effective medium approximation theory using thermal conductivity and density of water, and $CaCl_2$ at 25°C [50]. However, as the thermal conductivity of water and the saturated salt solution have a slight difference (maximum 8% for the saturated $CaCl_2$ solution), an approximate value of 0.6 $W \cdot m^{-1} \cdot K^{-1}$ is used in the model.

Though the temperature effect on the thermal conductivity of silica gel and $CaCl_2$ in the studied temperature range (20°C - 120°C) is negligible, the thermal conductivity of liquid water has a 0.08 $W \cdot m^{-1} \cdot K^{-1}$ increase (12%) in this temperature range. Further investigation indicates that this difference will result in a 0.7% increase in the thermal conductivity of the effective medium. Therefore, it can also be neglected to simplify the model.

As shown in Figure 2.9, an equivalent cubic diagonal of a spherical-shaped object is defined as the diagonal of a cube of equivalent volume. The equivalent cubic diagonal, d_{eq}, for the pore volume is calculated as:

$$d_c = 1.396 \cdot d_p \tag{21}$$

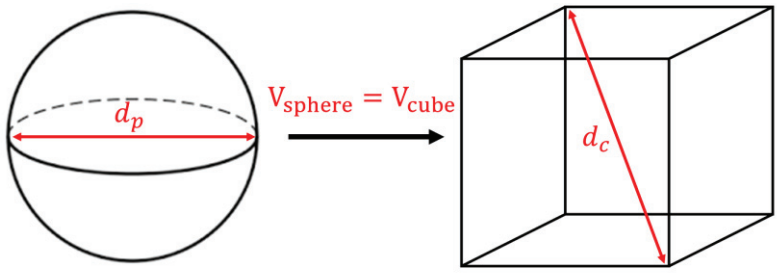

Figure 2.9. Schematic illustration of an equivalent cubic diagonal of a spherical-shaped object.

Based on the geometrical assumptions of the unit cell, the solid host matrix radius, r_s, is calculated by solving the following equation using porosity (ε), and d_c as follows:

$$\varepsilon = \frac{12\pi\sqrt{3}}{d_c^3} r_s^3 - \frac{9\pi}{d_c^2} r_s^2 + 1 \tag{22}$$

The absorbed water uptake layer thickness, t_w, is also calculated by solving the following equation using the true density of solid host matrix and water (ρ_s, ρ_w), ω, r_s, d_c as:

$$\omega = \frac{\rho_w}{\rho_s}\left(\frac{-t_w^3 + \left(\frac{3d_c}{4\sqrt{3}} - 3r_s\right)t_w^2 + \frac{3d_c r_s}{2\sqrt{3}}t_w}{\left(\frac{3d_c}{4\sqrt{3}} - r_s\right)r_s^2}\right) \quad (23)$$

Finally, based on the simplified thermal resistance network of the unit cell, the thermal conductivity of the effective medium of sorbent composite is calculated and simplified using MAPLE software as:

$$k_m = \frac{4\sqrt{3}/d_c}{\frac{\frac{d_c}{\sqrt{3}} - 2r_s}{1.2 \times t_w \cdot r_s} - \frac{1.2 \times \left[arctan\left(\frac{1.2 - k_s}{\sqrt{1.2k_s - k_s^2}}\right) - \pi\sqrt{1.2k_s - k_s^2}\right]}{t_w \cdot (k_s - 0.6)\sqrt{1.2k_s - k_s^2}}} \quad (24)$$

For this study, and generally, in the case of using silica gel B150 (B represents the particle size range of 200 to 500 μm, and 60 represents the average particle size reported by the supplier as 150 Å) as the host matrix, r_s and t_w can be calculated using the following correlations, which are derived for typical porosity range of silica gels (i.e., $0.4 < \varepsilon < 0.8$) and water uptake range of $0.01 < \omega < 0.99$ both fitted with the coefficient of determination of $r^2 = 0.99$.

$$r_s = -6.3\varepsilon + 7.3 \quad (25)$$

$$t_w = 2.4\omega \quad (26)$$

Using Eqs. (25) and (26) in Eq. (24) will further simplify the effective thermal conductivity medium as:

$$k_m = \frac{\omega(16.3 - 14\varepsilon) - 1.4\varepsilon + 2.8}{31.5 - 16\varepsilon} \quad (27)$$

To summarize the model development for the effective thermal conductivity of consolidated sorbent composites with conductive additive particles, an algorithm flow chart is designed and presented in Figure 2.10.

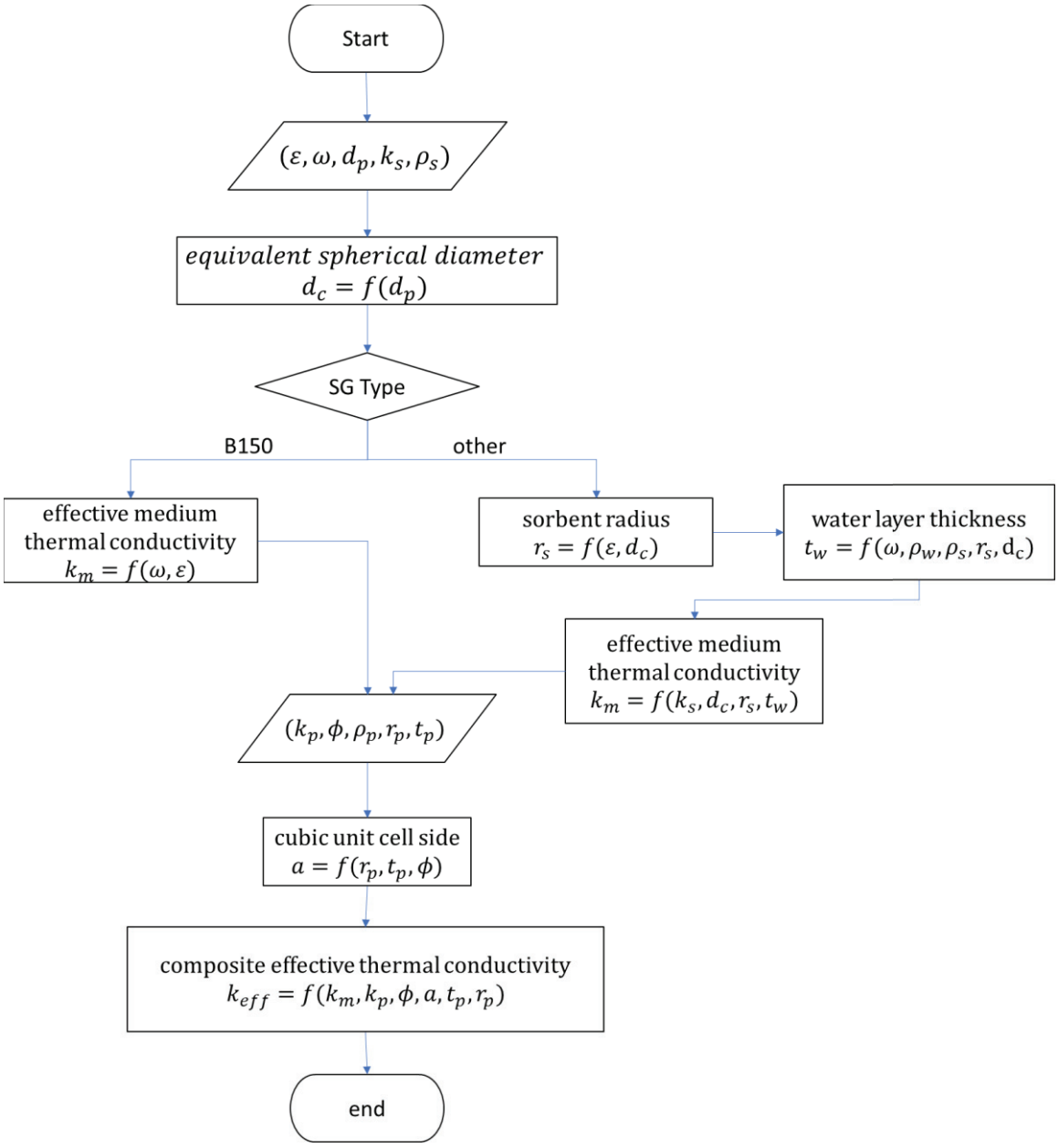

Figure 2.10. An algorithm flowchart for the present analytical model.

2.2.2. Thermal conductivity of the sorbent composite, including a conductive additive particle

Following the methodology introduced by Fayazmanesh et al. [45], the effective thermal conductivity of the sorbent composites containing conductive additive particles is calculated assuming that identical disk-shaped additive particles are evenly and randomly dispersed throughout the composite. The host matrix here is the modeled by an effective medium and the effective medium thermal conductivity (k_m), is calculated using the

correlations introduced in the previous Sub-section 2.2.1. In this way, the effect of water uptake, host matrix pore size distribution, porosity, and the additive particles are taken into account.

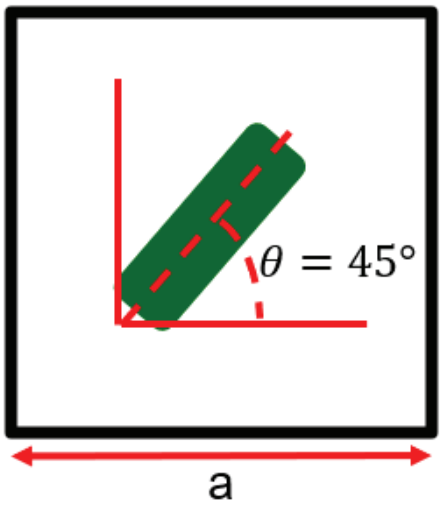

Figure 2.11. A schematic illustration of an effective medium composite with conductive additive particle cubic unit cell.

The size of the unit cell depends on the volume fraction of additive particles in each sample, and it is calculated using the additive particle dimensions, and the density of particles and effective medium. Therefore, the effective thermal conductivity of the consolidated sorbent composite for an additive particle with an angle of $\Theta = 45°$ will be:

$$k_{eff} = \frac{1}{2}\left[\frac{k_m\left[\frac{t_p.k_m}{\varphi} + (k_p - k_m)a\right]}{\frac{t_p.k_m}{\varphi} + (k_p - k_m)(a - t_p)} + \frac{r_p\left(2k_p a - \pi r_p(k_p - k_m)\right)}{r_p\left(k_m.(a^2 - 2r_p t_p)\cdot\left(2k_p a - \pi r_p(k_p - k_m)\right)\right) + 2t_p a}\right] \quad (28)$$

where, k_p, r_p, t_p are the thermal conductivity, and radius and thickness of the additive particle, respectively, and *a* is the side length of the cubic unit cell as shown in Figure 2.11. A schematic illustration of an effective medium composite with conductive additive particle cubic unit cell, and calculated as:

$$a = \sqrt[3]{\pi r_p^2 t_p / \varphi} \tag{29}$$

A MATLAB code is developed to calculate the thermal resistances, solve the equations, and estimate the effective thermal conductivity and thermal diffusivity of consolidated sorbent composites based on the algorithm shown in Figure 2.10 as a function of the measured input parameters.

Chapter 3. Experimental study

3.1. Sample preparation

Polyvinyl alcohol (PVA) binder (40,000 MW, Amresco Inc.) was dissolved in water; subsequently, $CaCl_2$ (Calcium Chloride C77-500, 4-20 mesh, anhydrous, Fisher Scientific), and silica gel (SiliaFlash® B150, Silicycle, Inc., Quebec, Canada) and different amounts of graphite flakes (808091, 99% Carbon, +100 mesh), consisting of both 150 μm fine particles and thin flakes up to 1.3 mm long, Sigma-Aldrich, or expanded natural graphite (Timrex C-Therm 002 Z11021), consisting of 81 μm particles, IMERYS, were added to the aqueous solution. The slurries were baked for one hour at 80°C and then heated to 180°C for one hour to cross-link the binder. Consolidated salt-in-matrix sorbent composites (shown in Figure 3.1) were prepared with 0-15 wt% of graphite flakes or 0-5 wt% of expanded natural graphite as thermally-conductive additives. The optimal microscopic image of graphite flakes and a SEM image of expanded natural graphite [5] are shown in Figure 3.3, and Figure 3.4, respectively. The composition and total mass of the sorbent composites prepared in this study are presented in Table 3.1. Scanning electron microscope (SEM) images of sorbent composites made with silica gel, $CaCl_2$, PVA (a) without a thermally-conductive additive; (b) with 20 wt.% graphite flakes; and (c) with 5 wt.% of expanded natural graphite are shown in Figure 3.2.

Table 3.1. Composition and total mass of sorbent composite samples.

Name	Silica gel (wt%)	$CaCl_2$ (wt%)	PVA (wt%)	Graphite flake (wt%)	ENG (wt%)	Dry mass (g)
CG0	45	45	10	0	0	7.54
CGF5	42.5	42.5	10	5	0	8.65
CGF10	40	40	10	10	0	8.60
CGF15	35	35	10	15	0	9.00
CENG1	44.5	44.5	10	0	1	10.54
CENG3	43.5	43.5	10	0	3	9.70
CENG5	42.5	42.5	10	0	5	10.80

Figure 3.1. **(a) Sorbent composites made with 1, 3, and 5 wt.% of ENG additive (CENG1, CENG3, CENG5); and (b) sorbent composites with 0, 5, 10, 15 wt. % of graphite flakes additive (CG0, CGF5, CGF10, CGF15).**

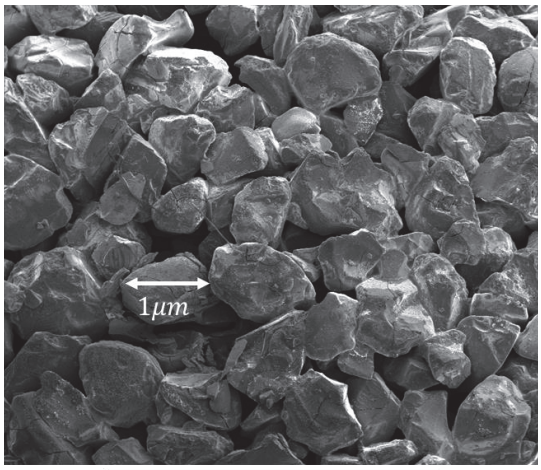

(a)

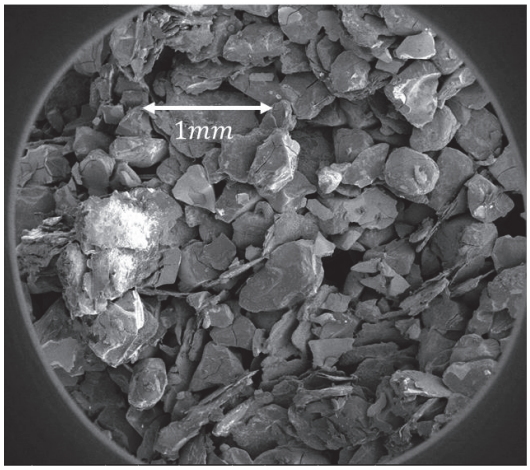

(b)

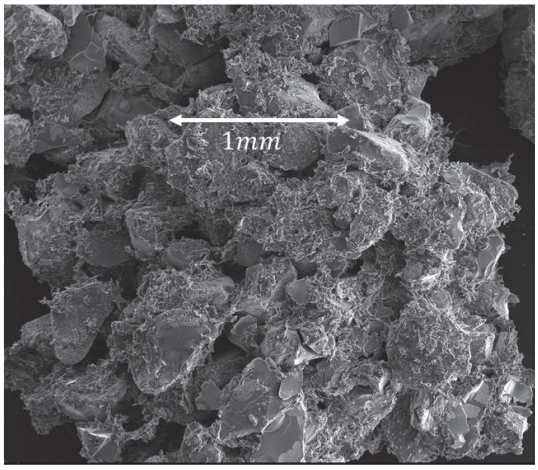

(c)

Figure 3.2. SEM images of: (a) a composite sorbent made with SG-$CaCl_2$-PVA without conductive additives; (b) a composite sorbent made with SG-$CaCl_2$-PVA with 20 wt.% of GF [9]; and (c) a composite sorbent made with SG-$CaCl_2$-PVA with 5 wt.% of ENG.

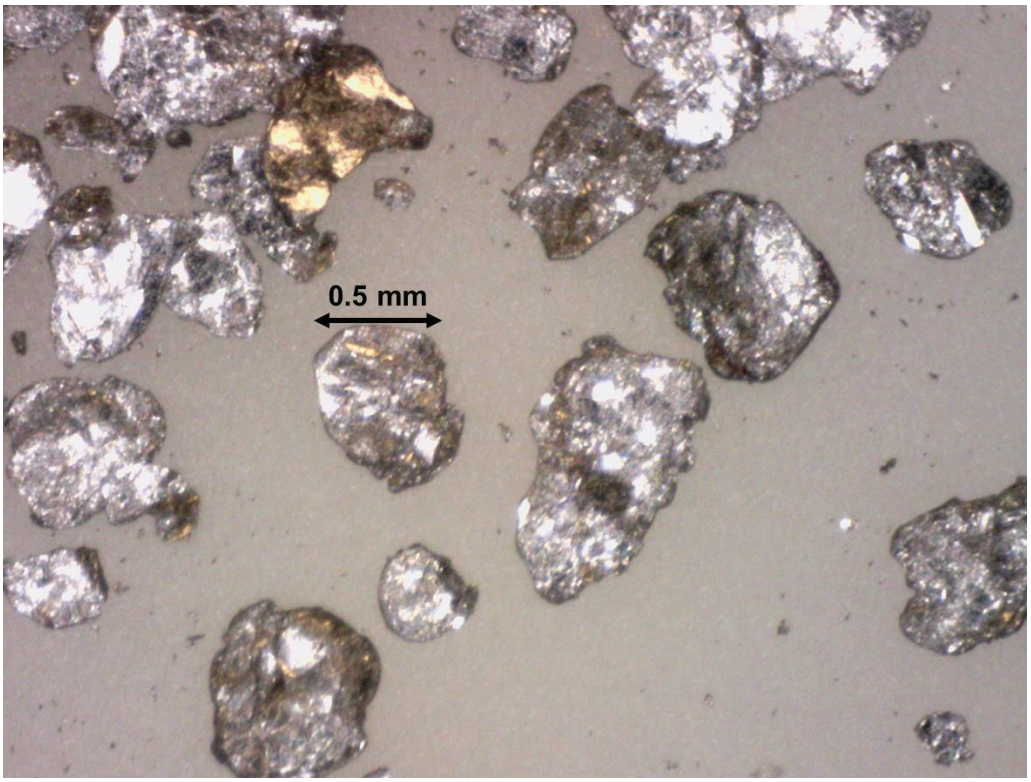

Figure 3.3. An optimal microscopic image of graphite flakes.

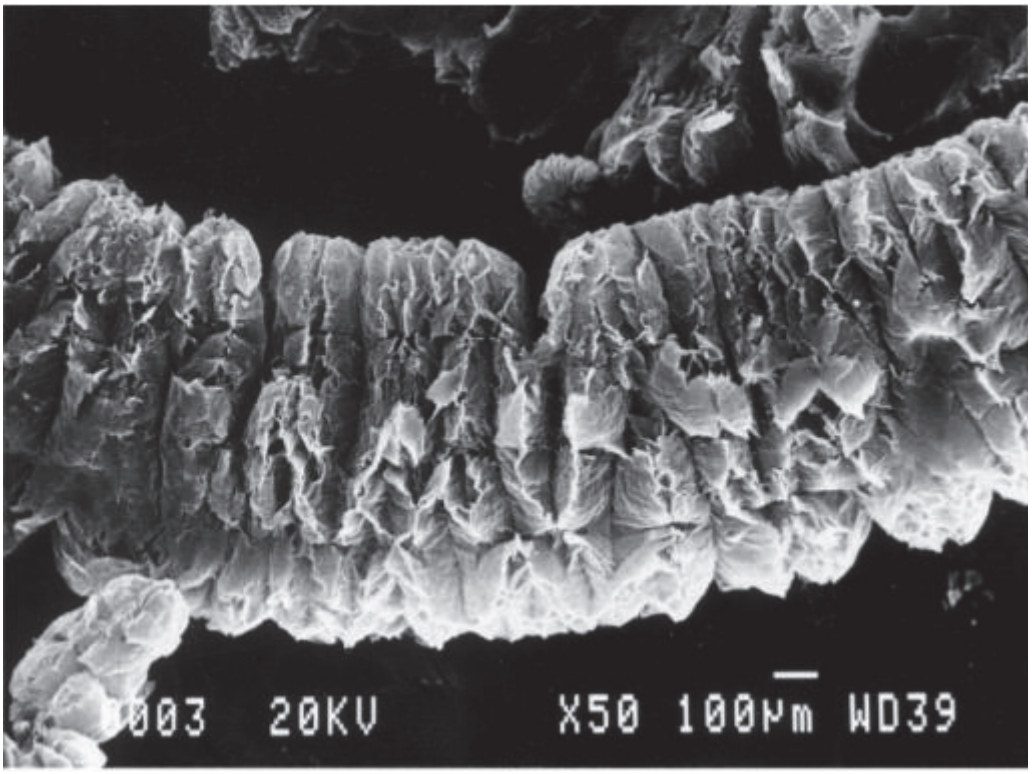

Figure 3.4. A SEM image of expanded natural graphite (ENG) [5].

3.2. Thermal conductivity and diffusivity measurement

A hot disk transient plane source thermal constant analyzer (TPS 2500S, ThermTest Inc., Fredericton, Canada) capable of the precise measurement of thermal conductivity, diffusivity, and specific heat was used for this study. This apparatus uses a transient plane source method following the ISO Standard 22007-2.2 [16]. The testbed measurement setup, including the sample assembly is schematically illustrated in Figure 3.5 and shown in Figure 3.6.

The instrument has different sensor types and software modules to perform bulk materials measurements (isotropic and anisotropic), thin films, powders, and liquids. In this study, a bulk sensor (7577) with a 2-mm diameter nickel double spiral insulated in a thin layer of Kapton is used for both transient heating of the sample and temperature measurements. Details of TPS testing can be found elsewhere [10][51]. A humidifier (P-10C-1C-2-0-031300-v7, Cellkraft AB, Sweden) was connected to the thermal constant analyzer to control the humidity inside the TPS chamber. Also, a heating/cooling circulator was connected to the chamber to maintain a constant controlled temperature.

For bulk material (isotropic) measurements, a sensor was placed on either side of a pair of dried identical samples. After 20 minutes for temperature and the specified RH humidity equilibration, measurements were performed on each sample five times at three different locations, and a standard deviation of 10% was measured.

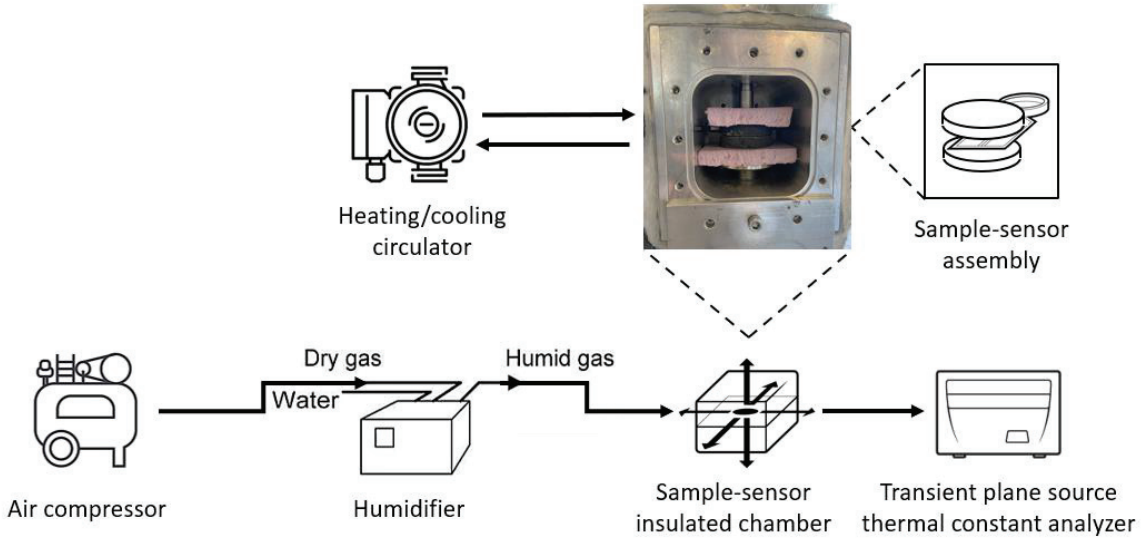

Figure 3.5. **A schematic of a testbed measurement setup, including an air compressor, humidifier, TPS analyzer instrument, heating/cooling circulators, and a sample-sensor assembly insulated chamber containing RH and temperature sensors.**

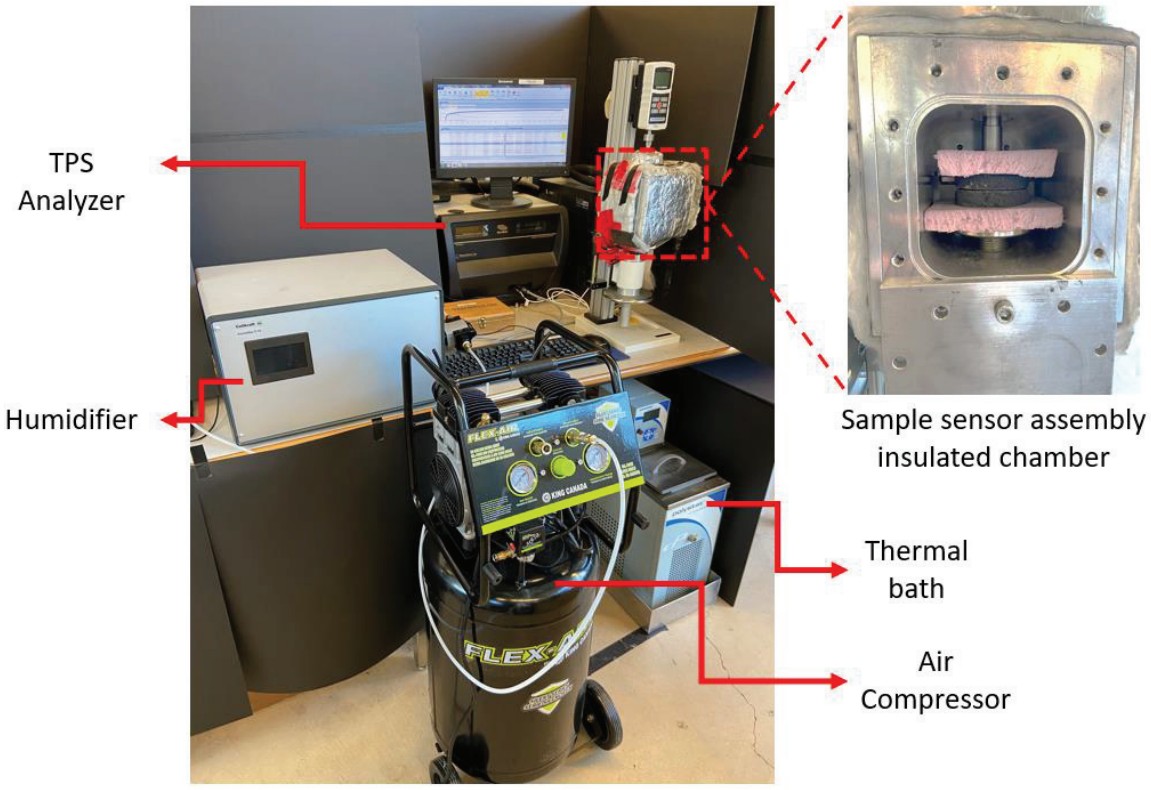

Figure 3.6. **A testbed measurement setup, including an air compressor, humidifier, TPS analyzer instrument, thermal bath, and a sample-sensor assembly insulated chamber containing RH and temperature sensors.**

3.3. Uncertainty analysis

Following the same methodology as [52], the uncertainty of thermal conductivity u_k was calculated as:

$$u_k = \sqrt{u_{k,m}^2 + \sigma_k^2} \tag{30}$$

where, $u_{k,m}$ is the measurement accuracy of the TPS instrument and σ_k is the standard deviation of the measurements. The value of $u_{k,m}$ reported by the manufacturer is 5% of the reading [53].

The uncertainty of diffusivity u_α was calculated identically to conductivity as:

$$u_\alpha = \sqrt{u_{\alpha,m}^2 + \sigma_\alpha^2} \tag{31}$$

where, $u_{\alpha,m}$ is set to be 5% of the reading and σ_α is the standard deviation of the measurements.

3.4. Geometrical parameters of the sorbent composite and additive particles

Geometrical parameters, including the host matrix pore size distribution, and graphite-based additive particle size should be measured to be used as input to the present model. Nitrogen sorption isotherms of the samples were collected with a volumetric physisorption analyzer (Autosorb iQ-MP, Quantachrome Instruments) to determine the average pore diameter (d_p) and pore volume (V). Prior to the testing, the samples were dried under vacuum at 150°C for 6 hours, followed by 2 hours at 200°C.

3.5. Porosity calculation

As sorbent composite porosity is one of the key parameters used in the model, the porosity of sorbent composite was calculated using the following methodology.

First, the bulk density of each sorbent composite is calculated using the dry mass ($m_{composite}$) and volume ($V_{composite}$) of disk-shaped sorbent sample.

$$\rho_{composite} = \frac{m_{composite}}{V_{composite}} = \frac{m_{composite}}{t_c \times \frac{\pi d_c^2}{4}} \tag{32}$$

where, t_c and d_c are the composite thickness and diameter, respectively.

Next, solid volume (V_{solid}) is measured based on the true densities and mass ratios of silica gel, $CaCl_2$, PVA, and additives as below. The true densities used in this model is presented in Table 3.2.

$$V_{solid} = \frac{m_{SG}}{\rho_{SG}} + \frac{m_{CaCl_2}}{\rho_{CaCl_2}} + \frac{m_{PVA}}{\rho_{PVA}} + \frac{m_{additive}}{\rho_{additive}} \tag{33}$$

Table 3.2. True densities of sorbent composite component materials.

Material	Silica gel	$CaCl_2$	PVA	Graphite flake
True density (g·cm^{-3})	2.4	2.15	1.19	2.26

Finally, the porosity of each sorbent composite is calculated using the solid volume and composite volume as:

$$\varepsilon = \frac{V_{composite} - V_{solid}}{V_{composite}} \tag{34}$$

3.6. Pore size distribution

The differential pore volume distribution of the silica and composite samples were obtained with the help of Dr. Claire McCague, a postdoctoral fellow at LAEC, through the analysis of the adsorption branch of the N_2 isotherms and shown in Figure 3.7. Based on the measured data, the average pore size diameter for silica gel B150 was calculated as d_p = 16.76 nm. This average pore size diameter was used as a baseline and was a critical

parameter to determine the dimensions of the effective medium unit cell of the present model. It would be also worthwhile to report that the median of pore size diameter, the total pore volume, and the surface area per gram were 17 nm, 1.127 $cm^3 \cdot g^{-1}$, and 268.13 $m^2 \cdot g^{-1}$, respectively.

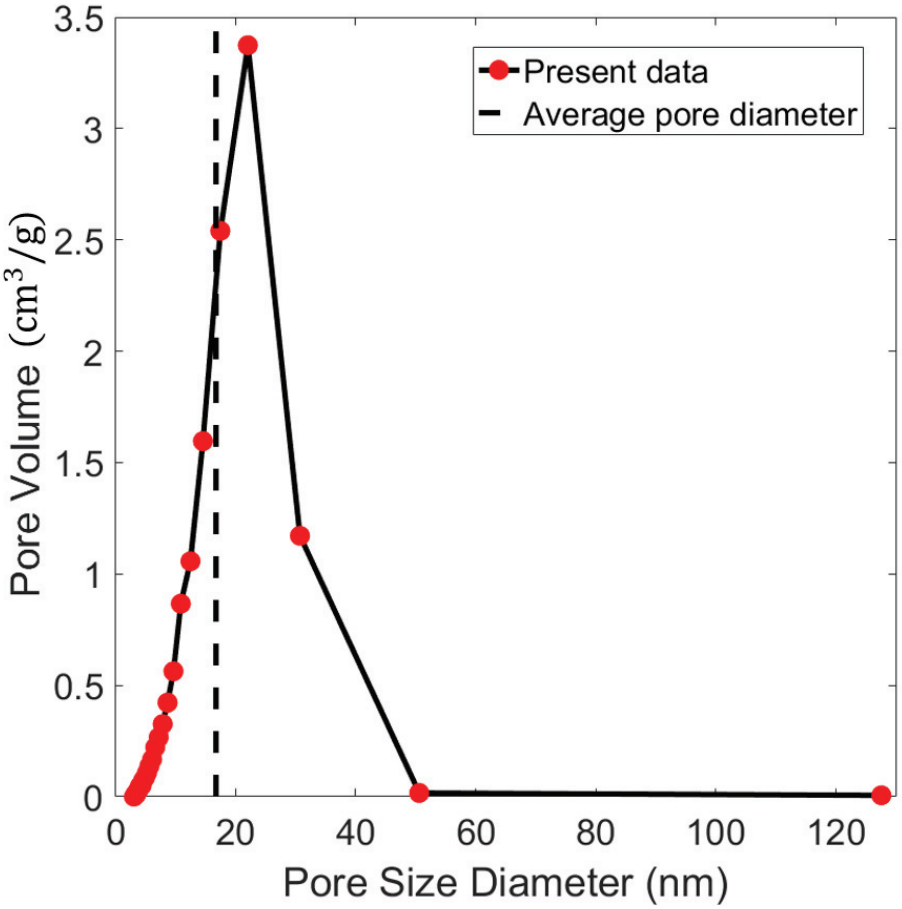

Figure 3.7. **The pore size distribution for silica gel B150 from N_2 adsorption isotherms was collected using a volumetric physisorption analyzer (Autosorb iQ-MP, Quantachrome Instruments) in our lab to determine the average pore diameter (d_p) and pore volume (V). The dashed line indicates the average pore diameter (d_p = 16.76 nm).**

Chapter 4. Model validation, parametric study, and sensitivity analysis

4.1. Model validation

The thermal conductivity of the effective medium is validated with experimental data collected in our lab for sorbent composites made of SG B150, $CaCl_2$, and PVA tested at a RH of 2-70%. As shown in Figure 4.1, the model can predict the thermal conductivity of the sorption composite and the increasing trend as a function of water uptake and shows a good agreement with the experimental data with the average and maximum relative differences of 5.72% and 10.66%, respectively.

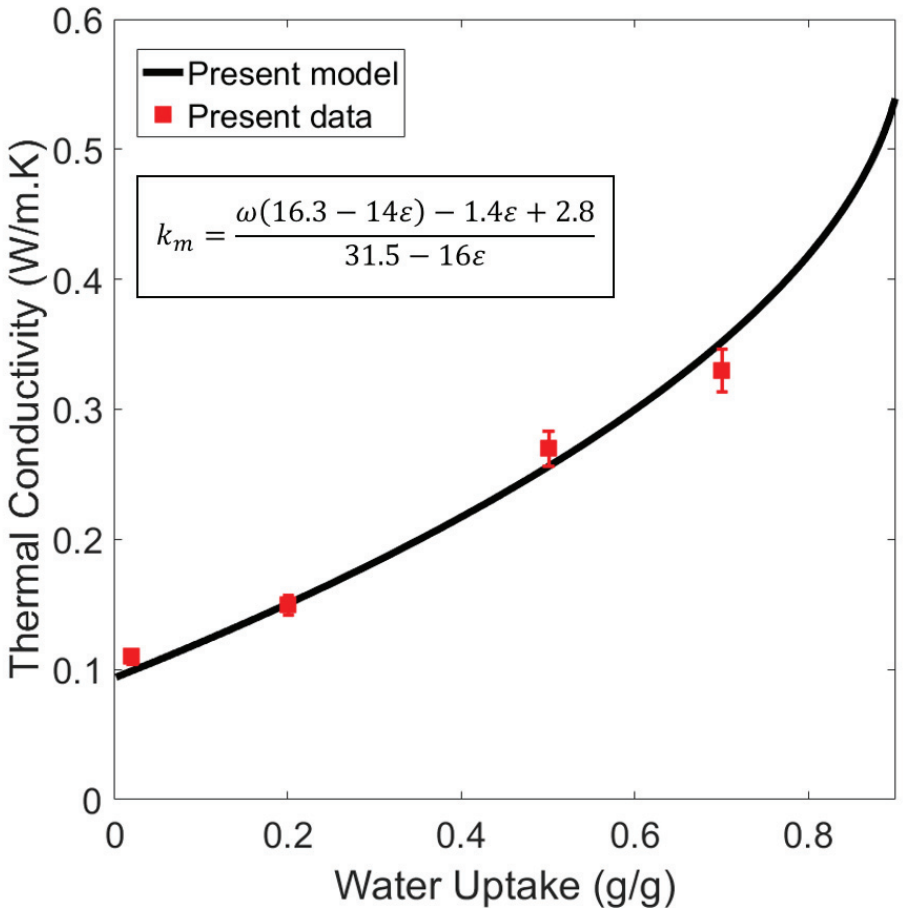

Figure 4.1. A comparison between the measured thermal conductivity and analytical model for the sorbent composite CG0, without thermally-conductive additives, over a water uptake range of 0.02 to 0.9 ($g \cdot g^{-1}$).

The present analytical model for the effective thermal conductivity of consolidated sorbent composites (SG B150, $CaCl_2$, and PVA) containing 0-15 wt.% of graphite flakes or 0-5 wt.% of expanded natural graphite are compared to the measured experimental data of the samples shown in Figure 4.2 and Figure 4.3, respectively. The analytical model can predict the experimental data rather well with a minimum, maximum and averaged relative difference between the model and data of 0.02%, 7.69%, and 4.15%, respectively.

A parametric study has been carried out to show the variation of the effective thermal conductivity of the sorbent composite with water uptake, sorbent porosity, additive type, and additive content. Sorbent material properties and geometrical parameters of the unit cell were considered as a baseline (shown in Table 4.1) in which each parameter is changed over an arbitrarily chosen range while other parameters were kept constant.

Table 4.1. Baseline parameters for the parametric study.

Sorbent composite	RH	ω ($g \cdot g^{-1}$)	Sorbent porosity	Additive type	φ (wt. %)
CGF0	2%	0.02	0.7	Graphite Flakes	0-15

4.2. Impact of additives on the effective thermal conductivity of sorbent composites

The graphite flakes and expanded natural graphite additives had different distributions in the composite samples, as well as different particle sizes, aspect ratios, and specifically, the order of magnitude difference in their bulk densities. Furthermore, the expanded natural graphite had a significantly more pronounced effect on the effective thermal conductivity of the consolidated sorbent composites. The thermal conductivity of the composite sorbents (CG0, CGF5, CGF10, CGF15) increased from 0.11 to 0.70 $W \cdot m^{-1} \cdot K^{-1}$ as the graphite flakes content was increased from 0 to 15 wt. % when tested with a RH of 2%, a ~ 536% enhancement shown in Figure 4.2. The addition of 5 wt. % of ENG to the composite sorbents (CG0, CENG1, CENG3, CENG5) also increased the thermal conductivity from 0.11 to 0.74 $W \cdot m^{-1} \cdot K^{-1}$ when tested with a RH of

2%, a ~ 572% enhancement shown in Figure 4.3. The comparison between the effect of GF and ENG as thermally conductive additives are also shown in Figure 4.4., indicating the more significant impact of ENG on the effective thermal conductivity of sorption composites. Nevertheless, , the low density of ENG poses some volumetric challenges like decreasing the specific cooling or heating power per volume and also adversely affects the mechanical strength of sorbent coatings.

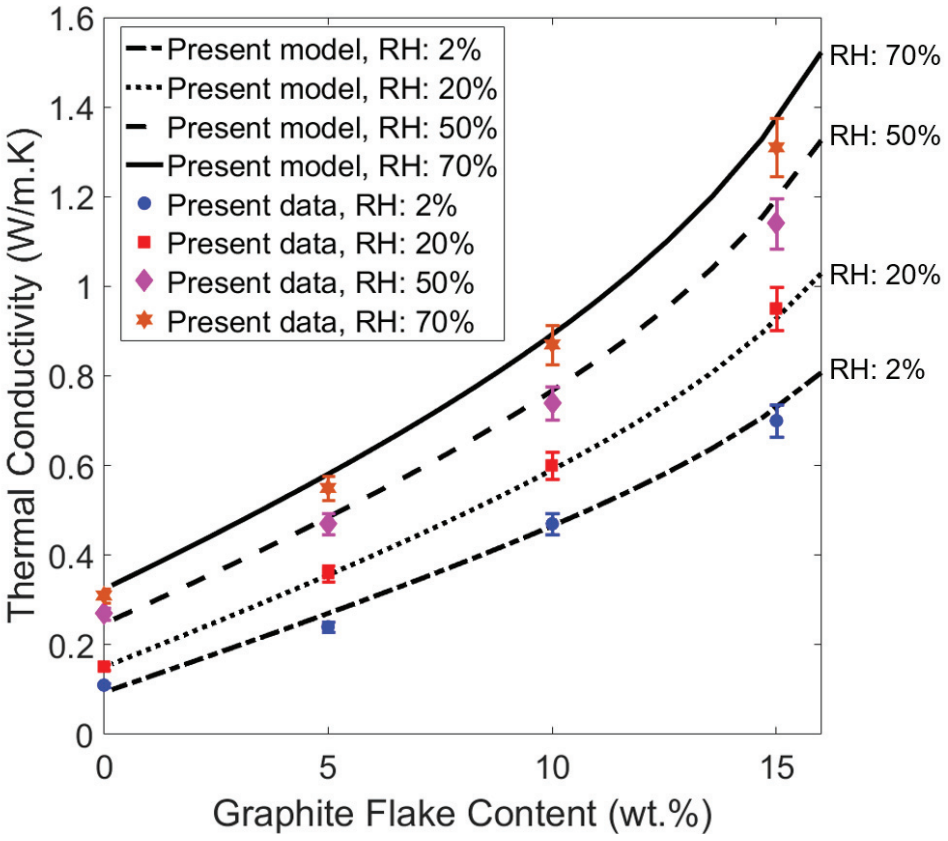

Figure 4.2. **A comparison between the measured thermal conductivity and analytical model for the consolidated sorbent composites CG0, CGF5, CGF10, CGF15. Samples were measured at 2, 20, 50 and 70% RH.**

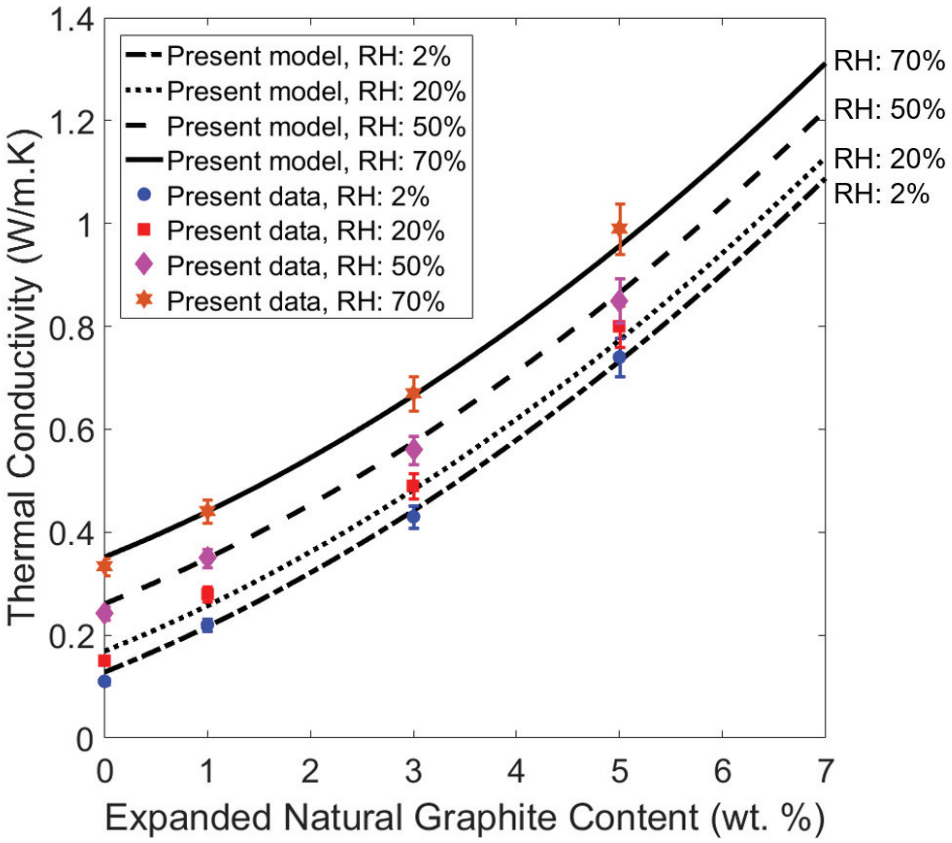

Figure 4.3. **A comparison between the measured thermal conductivity and analytical model for the consolidated sorbent composites CG0, CENG1, CENG3, CENG5. Samples were measured at 2, 20, 50 and 70% RH.**

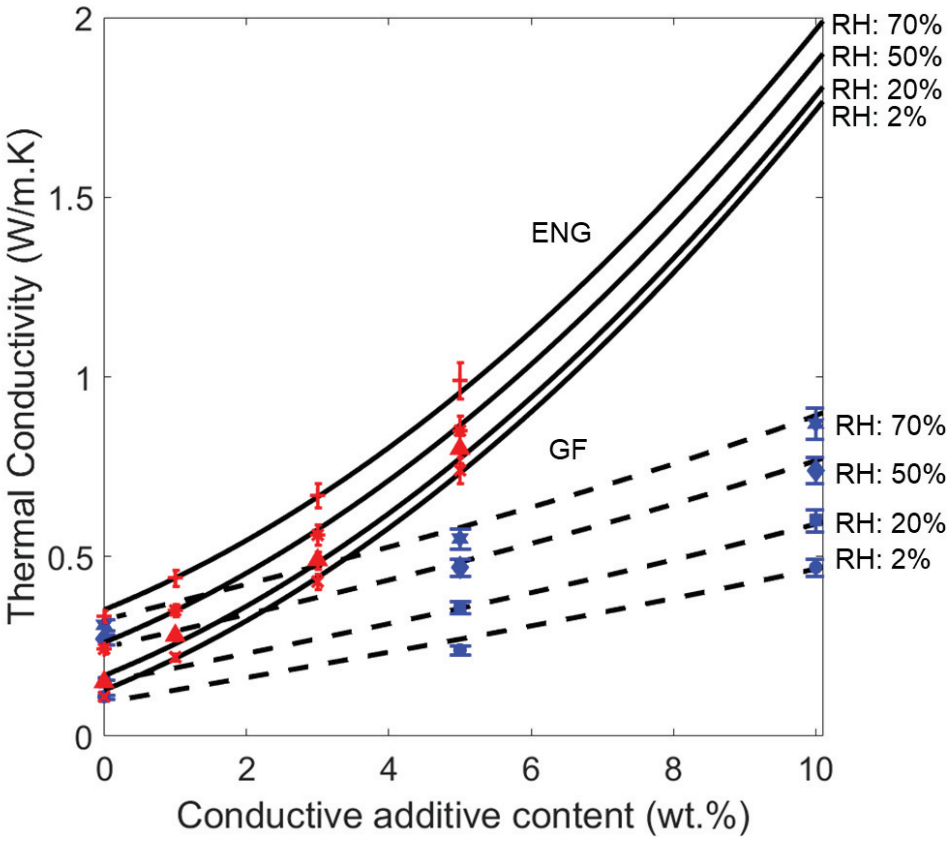

Figure 4.4. **A comparison between the effect of graphite flakes and expanded natural graphite on the effective thermal conductivity of the consolidated sorbent composites samples at 2, 20, 50 and 70% RH.**

4.3. Impact of water uptake and additives on the thermal diffusivity of sorbent composites

To investigate the effects of water uptake and additive on the thermal diffusivity (α) of the sorbent composites, the thermal diffusivity of SG, $CaCl_2$, PVA composites were made with 0 to 15 wt.% of graphite flakes has been modeled using the following equation and compared with the sample's measurements in Figure 4.5.

$$\alpha = \frac{k}{\rho \cdot c_p} \tag{35}$$

where, ρ is the sorbent composite bulk density and c_p is the specific heat capacity.

The thermal diffusivity of the composite sorbents (namely, CG0, CGF5, CGF10, and CGF15) increased from 0.12 to 0.90 $mm^2 \cdot s^{-1}$ as the graphite flake content was increased from 0 to 15 wt.% when tested with a RH of 2%, an 650% enhancement. This significant increase occurs because adding additive content not only increases the effective thermal conductivity of the consolidated composite, but also decreases the bulk density and specific heat capacity of the composite.

On the other hand, though increasing water uptake raises the effective thermal conductivity of the sorbent composite, it also increases the bulk density and specific heat capacity of the composite which eventually leads to a less significant increase in the thermal diffusivity. Therefore, as the water uptake was increased from 0.02 to 0.9 ($g \cdot g^{-1}$) for the sorbent composite CGF15 with a 15 wt.% of graphite flakes, the thermal diffusivity of the sorbent composites increased from 0.90 to 1.20 $mm^2 \cdot s^{-1}$, a ~33% enhancement.

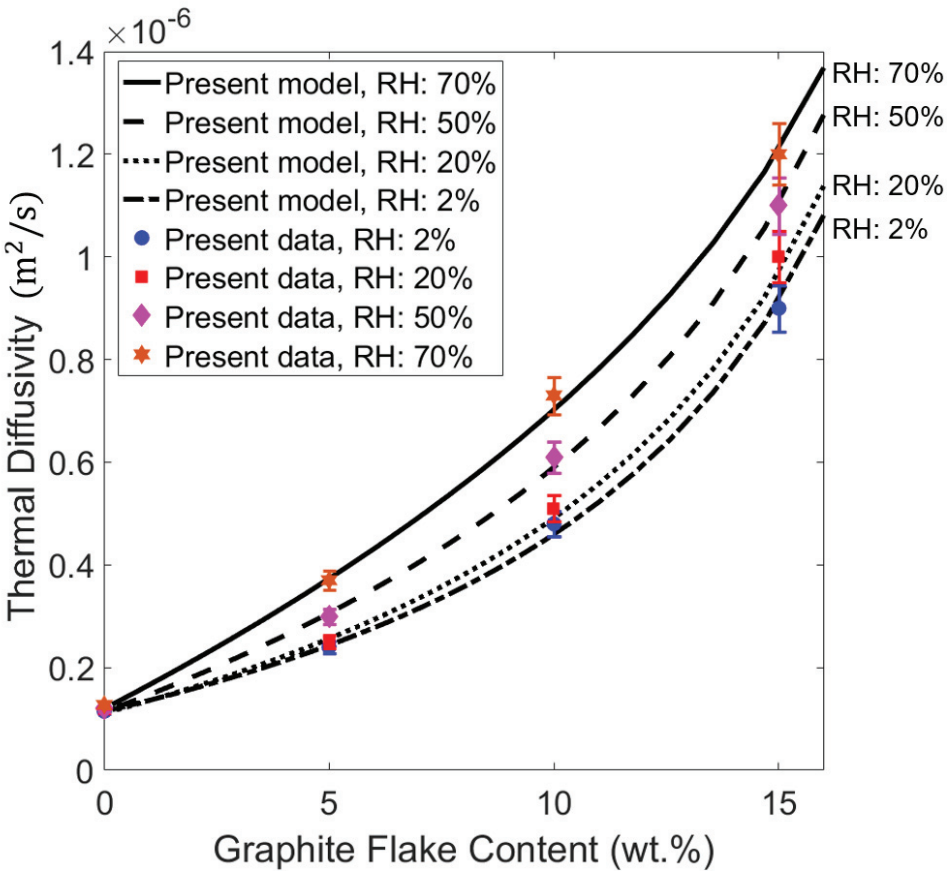

Figure 4.5. **A comparison between the measured thermal diffusivity and analytical model for consolidated sorbent composites CG0, CGF5, CGF10, CGF15. Samples were measured at 2, 20, 50, and 70% RH.**

4.4. Water uptake impact on the effective thermal conductivity of sorbent composites

In order to investigate the impact of water uptake on the effective thermal conductivity of the sorbent composite, the effective thermal conductivity of SG, $CaCl_2$, PVA composites made with 0 to 15 wt.% of graphite flakes has been modeled and shown in Figure 4.6. The thermal conductivity of the composite sorbent CG0 increased from 0.11 to 0.46 $W \cdot m^{-1} \cdot K^{-1}$ as the water uptake was increased from 0.02 to 0.9 ($g \cdot g^{-1}$) for the sorbent with 0 wt. % of graphite flakes, a n~ 318% enhancement.

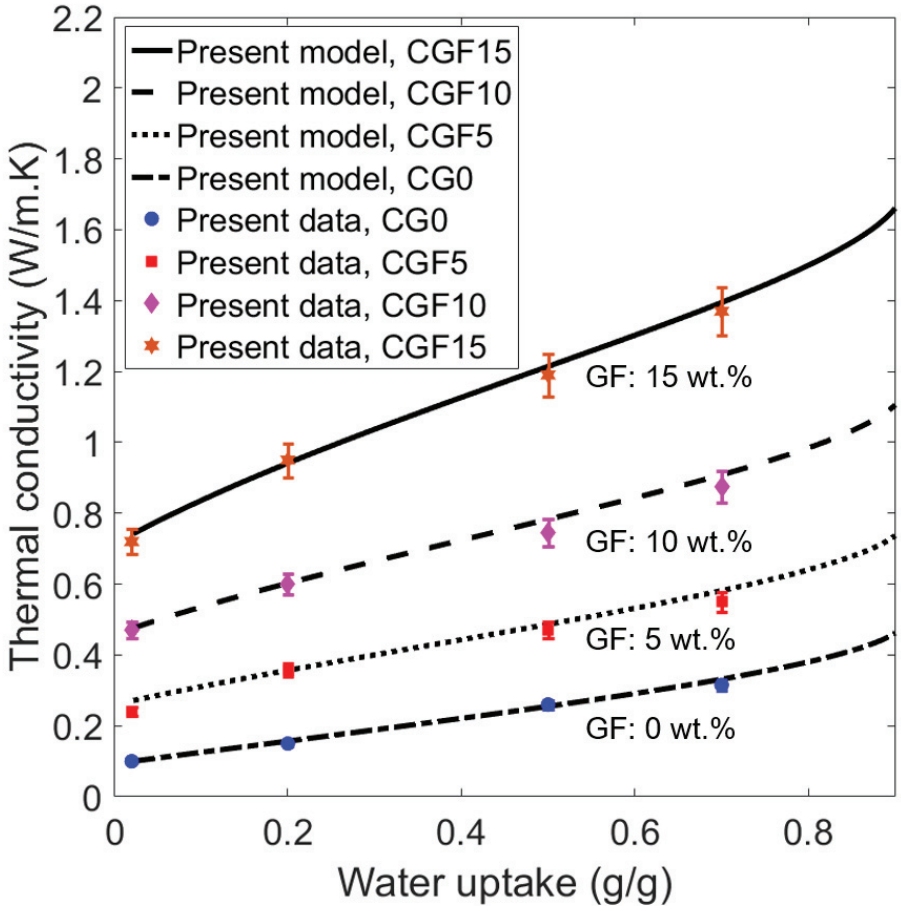

Figure 4.6. **The water uptake variation impact on the effective thermal conductivity of consolidated sorbents CG0, CGF5, CGF10, and CGF15.**

4.5. Impact of porosity on the effective thermal conductivity of sorbent composites

After the model is validated with several data sets, we can use the present model with a degree of confidence to predict the impact of other key parameters, such as silica gel porosity on the effective thermal conductivity of the sorbent composite, the effective thermal conductivity of SG, $CaCl_2$, PVA composites made with 0 to 15 wt.% of graphite

flakes has been modeled and shown in Figure 4.7. The thermal conductivity of the composite sorbent CG0 increased from 0.03 to 0.41 $W \cdot m^{-1} \cdot K^{-1}$ as the porosity was decreased from 80% to 40% for the sorbent with 0 wt.% of graphite flakes at 2% RH, a ~ 1200% enhancement. Nevertheless, it is important to note that decreasing porosity, depending on the case, can reduce the water uptake, which adversely impacts the sorption kinetics. Therefore, performing optimization is necessary to choose the porosity of silica gel.

The porosity of the sorbent composites CG0, CGF5, CGF10, and CGF15 are calculated based on their measured bulk densities and weight percentage and the true density of silica, $CaCl_2$, PVA, and graphite flakes in each composite.

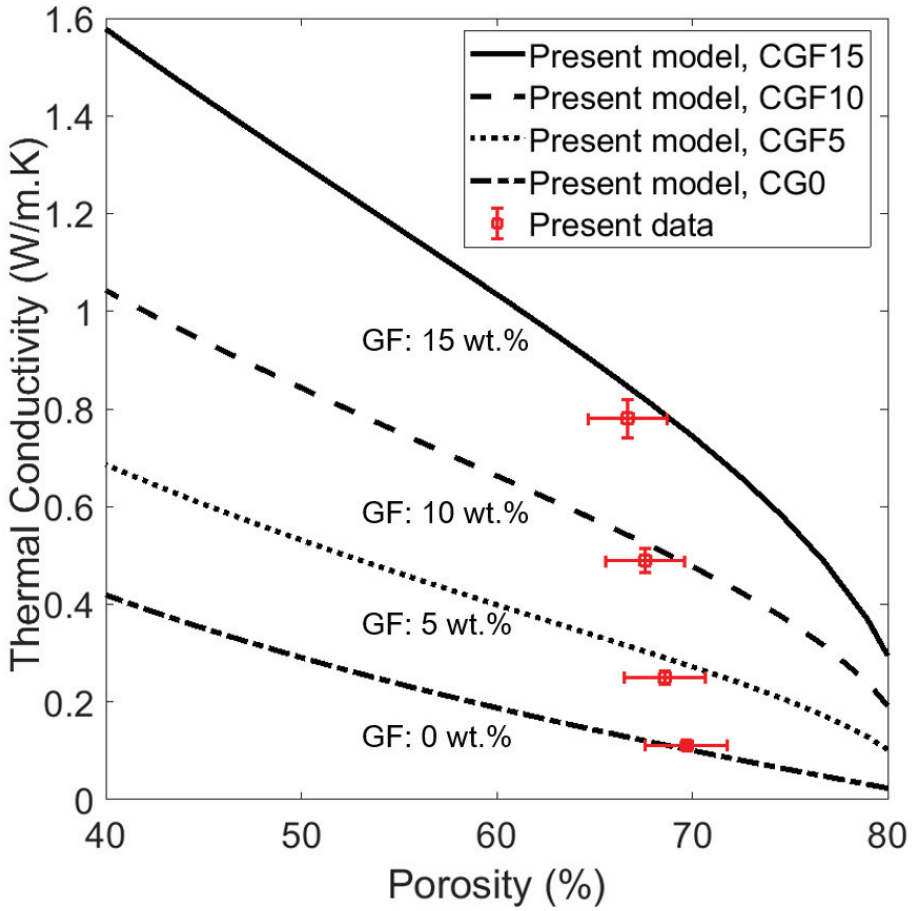

Figure 4.7. The porosity variation impact on the effective thermal conductivity of consolidated sorbents CG0, CGF5, CGF10, and CGF15, when tested with a 2% RH.

4.6. Sensitivity analysis of host matrix input parameters

As stated previously, this model was developed for silica gel-based composites, however; the proposed methodology can be extended and applied to sorption composites made with other sorts of host matrix as well. To do so, some thermophysical input parameters of that specific host matrix must be measured and given to the model. These parameters include thermal conductivity, true density, and porosity of the host matrix.

In order to have a better understanding of these input parameters and their influence on the effective thermal conductivity of the sorption composite, a sensitivity analysis is performed to clarify the research direction for developing other sorption composites with an enhanced thermal performance.

Figure 4.8. shows the sensitivity analysis of the effect of host matrix true density on the effective thermal conductivity of sorption composites. The results for three different host matrix true densities from 1200 to 4800 kg/m^3 indicates that increasing the host matrix true density will enhance the thermal conductivity of the sorbent composite. Though, it will cause more dead weight to the sorption system which will decrease the specific heating/cooling power per mass of the system.

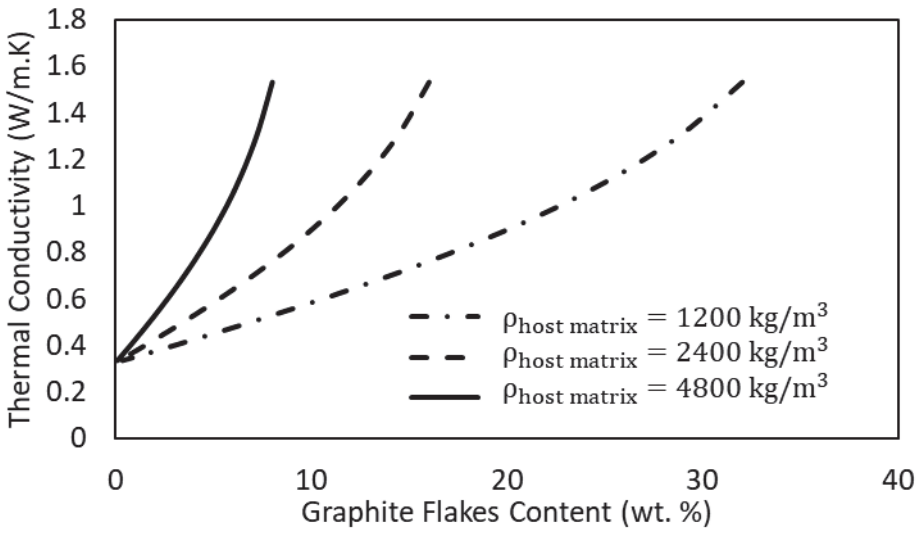

Figure 4.8. Sensitivity analysis of the impact of host matrix true density on the effective thermal conductivity of sorption composites.

Figure 4.9. shows the sensitivity analysis of the effect of host matrix porosity on the effective thermal conductivity of sorption composites. The results for porosity range of

0.4 to 0.8 indicates the enhancement of the effective thermal conductivity of the sorbent composite with decreasing the host matrix porosity. This happens because of the significantly lower thermal conductivity of water vapor in the pores comparing to the slod host matrix and liquid water. However, decreasing the host matrix porosity, depending on the case, may adversely affect the sorption capacity of the system.

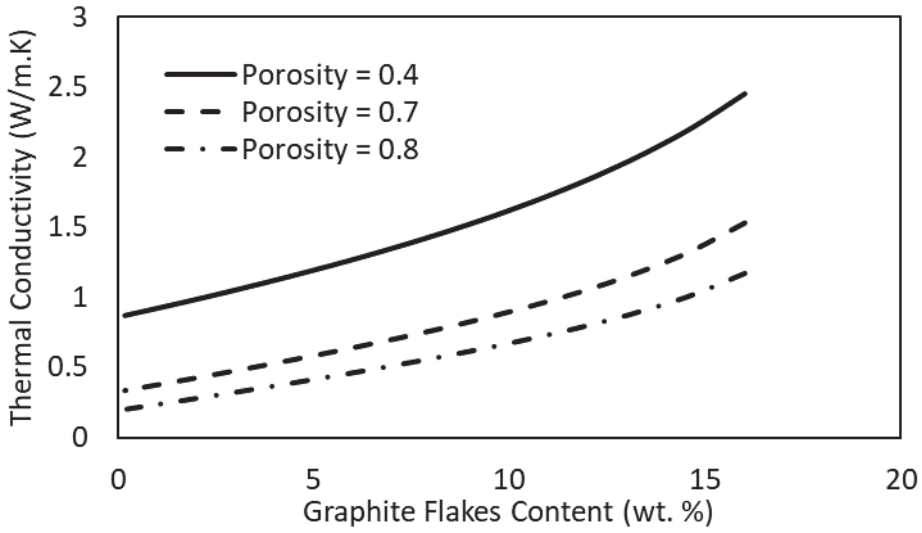

Figure 4.9. Sensitivity analysis of the impact of host matrix porosity on the effective thermal conductivity of sorption composites.

Figure 4.10. shows the sensitivity analysis of the effect of host matrix thermal conductivity on the effective thermal conductivity of sorption composites. The results for host matrix thermal conductivity range of 1.35 to 10.35 $W \cdot m^{-1} \cdot K^{-1}$ for a sorbent composite with 70% porosity indicates the impact of host matrix thermal conductivity on the effective thermal conductivity of sorption composites. Based on the above-mentioned sensitivity analysis, a multi-objective optimization of the host matrix thermophysical input parameters is needed to find the optimum balance between the thermal performance and sorption kinetics of the system.

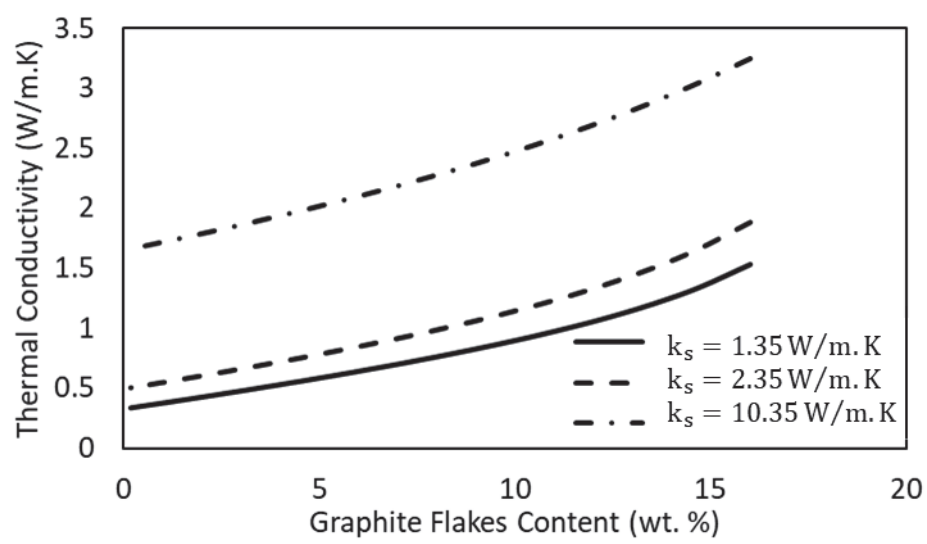

Figure 4.10. Sensitivity analysis of the impact of host matrix thermal conductivity on the effective thermal conductivity of sorption composites.

Chapter 5.

Conclusion, limitations, and scope for future work

5.1. Conclusion

A new analytical closed-form model has been developed that considers all salient morphological parameters, material properties, and operating conditions. This included thermal conductivity, specific heat capacity, and density of the sorbent and additive materials, host matrix pore size distribution, porosity, thermally-conductive additive type and content, water uptake, and temperature to predict the effective thermal conductivity and thermal diffusivity of the consolidated sorbent composite under the normal operating conditions of an adsorption or absorption system. This model was developed for silica gel-based composites; however, the proposed methodology can be extended and applied to other sorts of sorption composites as well.

Several consolidated salt-in-matrix sorbents were fabricated with silica gel, $CaCl_2$, PVA binder, and 0-15 wt.% of graphite flakes and with 0-5 wt.% of expanded natural graphite as thermally-conductive additives. The model has been successfully validated with the measured thermal conductivity of our sorbent samples collected at 25°C with 2, 20, 50, and 70% RH.

The results showed that the addition of 15 wt.% of graphite flakes or 5 wt.% of expanded natural graphite into consolidated sorbents lead to a 536% (from 0.11 to 0.70 $W \cdot m^{-1} \cdot K^{-1}$) and a 572% (from 0.11 to 0.74 $W \cdot m^{-1} \cdot K^{-1}$) increase in thermal conductivity, respectively, when tested at 2% RH and 25°C. It was also shown that the thermal conductivity of the composite sorbent CG0 increased from 0.11 to 0.46 $W \cdot m^{-1} \cdot K^{-1}$ (a ~ 318% enhancement) as the water uptake was increased from 0.02 to 0.9 ($g \cdot g^{-1}$).

Furthermore, a comprehensive parametric study was performed investigating the impact of water uptake, porosity, pore size, thermally conductive additive type, and additive content on the effective thermal conductivity and thermal diffusivity of the consolidated sorbent composite. This study showed that the thermal diffusivity of the composite sorbents (CG0, CGF5, CGF10, CGF15) increased from 0.12 to 0.90 $mm^2 \cdot s^{-1}$

as the graphite flake content was increased from 0 to 15 wt.% when tested with a RH of 2%, i.e., an 650% improvement.

The proposed analytical model shows good agreement with experimental data with the average and maximum relative differences of 4.15% and 7.69%, respectively. It provides a mechanistic and easy-to-use relationship that can be used as a design and optimization tool to enhance kinetics, heat transfer and overall performance of sorption systems.

5.2. Scope for future work

The recommendations for potential future research directions for this study are listed in the following:

- Perform a multi-objective optimization of the key parameters to maximize the effective thermal conductivity and thermal diffusivity of sorbent composites using the pareto frontier methodology;
- Investigate the impact of host matrix particle grain size (with or without same porosity) on the effective thermal conductivity of sorbent composites. It is also helpful to study the ratio of host matrix particle size to additive particle size;
- Implement the present analytical model on sorbent composites made with other host matrix materials, such as zeolite. For the new composite, morphological and thermophysical properties should be measured;
- Perform a sensitivity analysis for the impact of the additive particles' aspect ratio and shape on the effective thermal conductivity of the consolidated composite;
- Investigate the effect of adding two or more thermally conductive additives to the sorbent composites; and

- The proposed methodology in this Master's project can be applied to other porous medium composites of other applications including heat sinks, medical devices, hot spot removal, and regulating the temperature in variety of thermal systems.

References

[1] "IEA (2018), The Future of Cooling, IEA," *International Energy Agency*, 2018. [Online]. Available: https://www.iea.org/reports/the-future-of-cooling. [Accessed: 19-Apr-2021].

[2] "Net zero by 2050 plan for energy sector is coming – Analysis - IEA." [Online]. Available: https://www.iea.org/commentaries/net-zero-by-2050-plan-for-energy-sector-is-coming. [Accessed: 27-Apr-2021].

[3] J. M. Pinheiro, S. Salústio, J. Rocha, A. A. Valente, and C. M. Silva, "Adsorption heat pumps for heating applications," *Renewable and Sustainable Energy Reviews*, vol. 119. Elsevier Ltd, p. 109528, 01-Mar-2020.

[4] F. Meunier, "Adsorptive cooling: a clean technology," *Clean Prod. Process.*, vol. 3, no. 1, pp. 0008–0020, Jun. 2001.

[5] T. H. Eun, H. K. Song, J. Hun Han, K. H. Lee, and J. N. Kim, "Enhancement of heat and mass transfer in silica-expanded graphite composite blocks for adsorption heat pumps: Part I. Characterization of the composite blocks," *Int. J. Refrig.*, vol. 23, no. 1, pp. 64–73, Jan. 2000.

[6] K. Wang, J. Y. Wu, R. Z. Wang, and L. W. Wang, "Effective thermal conductivity of expanded graphite-CaCl2 composite adsorbent for chemical adsorption chillers," *Energy Convers. Manag.*, vol. 47, no. 13–14, pp. 1902–1912, Aug. 2006.

[7] X. Zheng, L. W. Wang, R. Z. Wang, T. S. Ge, and T. F. Ishugah, "Thermal conductivity, pore structure and adsorption performance of compact composite silica gel," *Int. J. Heat Mass Transf.*, vol. 68, pp. 435–443, Jan. 2014.

[8] A. A. Askalany, S. K. Henninger, M. Ghazy, and B. B. Saha, "Effect of improving thermal conductivity of the adsorbent on performance of adsorption cooling system," *Appl. Therm. Eng.*, vol. 110, pp. 695–702, Jan. 2017.

[9] H. Bahrehmand, M. Khajehpour, and M. Bahrami, "Finding optimal conductive additive content to enhance the performance of coated sorption beds: An experimental study," *Appl. Therm. Eng.*, vol. 143, no. July, pp. 308–315, 2018.

[10] K. Fayazmanesh, C. McCague, and M. Bahrami, "Consolidated adsorbent containing graphite flakes for heat-driven water sorption cooling systems," *Appl. Therm. Eng.*, vol. 123, pp. 753–760, 2017.

[11] Y. Y. Tanashev, A. V. Krainov, and Y. I. Aristov, "Thermal conductivity of composite sorbents 'salt in porous matrix' for heat storage and transformation," *Appl. Therm. Eng.*, vol. 61, no. 2, pp. 401–407, 2013.

[12] M. Tatlier, B. Tantekin-Ersolmaz, and A. Erdem-Şenatalar, "A novel approach to

enhance heat and mass transfer in adsorption heat pumps using the zeolite-water pair," *Microporous Mesoporous Mater.*, vol. 27, no. 1, pp. 1–10, Jan. 1999.

[13] M. Pons and Y. Feng, "Characteristic parameters of adsorptive refrigeration cycles with thermal regeneration," *Appl. Therm. Eng.*, vol. 17, no. 3, pp. 289–298, Mar. 1997.

[14] H. T. Chua, K. C. Ng, A. Malek, T. Kashiwagi, A. Akisawa, and B. B. Saha, "Modeling the performance of two-bed, silica gel-water adsorption chillers," *Int. J. Refrig.*, vol. 22, no. 3, pp. 194–204, May 1999.

[15] L. Marletta, G. Maggio, A. Freni, M. Ingrasciotta, and G. Restuccia, "A non-uniform temperature non-uniform pressure dynamic model of heat and mass transfer in compact adsorbent beds," *Int. J. Heat Mass Transf.*, vol. 45, no. 16, pp. 3321–3330, May 2002.

[16] ISO 22007, "INTERNATIONAL STANDARD conductivity and thermal diffusivity — ," *Int. Stand. ISO 22007-12017(E)*, vol. 2017, 2017.

[17] I. Energy Agency, "Statistics report Key World Energy Statistics 2020," 2020.

[18] D. Ürge-Vorsatz, L. F. Cabeza, S. Serrano, C. Barreneche, and K. Petrichenko, "Heating and cooling energy trends and drivers in buildings," *Renewable and Sustainable Energy Reviews*, vol. 41. Elsevier Ltd, pp. 85–98, 01-Jan-2015.

[19] W. Goetzler, R. Zogg, J. Young, and C. Johnson, "Alternatives to Vapor-Compression HVAC Technology Problems with Current Refrigerants," 2014.

[20] J. L. Chin and others, "State-of-the-Art Technologies on Low-Grade Heat Recovery and Utilization in Industry," *Chapters*, 2019.

[21] C. Forman, I. K. Muritala, R. Pardemann, and B. Meyer, "Estimating the global waste heat potential," *Renewable and Sustainable Energy Reviews*, vol. 57. Elsevier Ltd, pp. 1568–1579, 01-May-2016.

[22] N. C. Srivastava and I. W. Eames, "A review of adsorbents and adsorbates in solid-vapour adsorption heat pump systems," *Appl. Therm. Eng.*, vol. 18, no. 9–10, pp. 707–714, Sep. 1998.

[23] N. C. Srivastava and I. W. %J A. thermal engineering Eames, "A review of adsorbents and adsorbates in solid–vapour adsorption heat pump systems," vol. 18, no. 9–10, pp. 707–714, 1998.

[24] A. S. Ülkü and M. Mobedi, "Adsorption in energy storage," in *Energy Storage Systems*, Springer, 1989, pp. 487–507.

[25] H. Bahrehmand and M. Bahrami, "Development of novel sorber bed heat exchangers for sorption cooling systems," *PhD thesis*, 2020.

[26] H. Demir, M. Mobedi, and S. Ülkü, “The use of metal piece additives to enhance heat transfer rate through an unconsolidated adsorbent bed,” *Int. J. Refrig.*, vol. 33, no. 4, pp. 714–720, Jun. 2010.

[27] S. Yang, H. Kim, S. Narayanan, I. S. McKay, and E. N. Wang, “Dimensionality effects of carbon-based thermal additives for microporous adsorbents,” *Mater. Des.*, vol. 85, pp. 520–526, Nov. 2015.

[28] L. F. Cabeza, A. Solé, and C. Barreneche, “Review on sorption materials and technologies for heat pumps and thermal energy storage,” *Renew. Energy*, vol. 110, pp. 3–39, Sep. 2017.

[29] S. Mauran, P. Prades, and F. L’Haridon, “Heat and mass transfer in consolidated reacting beds for thermochemical systems,” *Heat Recover. Syst. CHP*, vol. 13, no. 4, pp. 315–319, Jul. 1993.

[30] J. J. Guilleminot, J. B. Chalfen, and A. Choisier, “Guilleminot: Heat and mass transfer characteristics... - Google Scholar,” in *Heat and Mass Transfer Characteristics of Composites for Adsorption Heat Pumps*, 1994.

[31] L. Pino, Y. Aristov, G. Cacciola, and G. Restuccia, “Composite materials based on zeolite 4A for adsorption heat pumps,” *Adsorption*, vol. 3, no. 1, pp. 33–40, Mar. 1997.

[32] Y. I. Aristov, G. Restuccia, G. Cacciola, and M. M. Tokarev, “Selective water sorbents for multiple applications, 7. Heat conductivity of CaCl2 - SiO2 composites,” *React. Kinet. Catal. Lett.*, vol. 65, no. 2, pp. 277–284, 1998.

[33] J. J. Healy, J. J. de Groot, and J. Kestin, “The theory of the transient hot-wire method for measuring thermal conductivity,” *Phys. B+C*, vol. 82, no. 2, pp. 392–408, Apr. 1976.

[34] A. Freni, M. M. Tokarev, G. Restuccia, A. G. Okunev, and Y. I. Aristov, “Thermal conductivity of selective water sorbents under the working conditions of a sorption chiller,” *Appl. Therm. Eng.*, vol. 22, no. 14, pp. 1631–1642, Oct. 2002.

[35] G. Buonanno and A. Carotenuto, “The effective thermal conductivity of a porous medium with interconnected particles,” *Int. J. Heat Mass Transf.*, vol. 40, no. 2, pp. 393–405, Jan. 1997.

[36] A. J. H. McGaughey and M. Kaviany, “Thermal conductivity decomposition and analysis using molecular dynamics simulations Part II. Complex silica structures,” *Int. J. Heat Mass Transf.*, vol. 47, no. 8–9, pp. 1799–1816, Apr. 2004.

[37] X. Lu, Y. Zhao, G. Wang, and X. Zhu, “Effects of structure characteristics and fluid on the effective thermal conductivity of sintered copper foam,” *Results Phys.*, vol. 19, p. 103655, Dec. 2020.

[38] B. Dawoud, M. I. Sohel, A. Freni, S. Vasta, and G. Restuccia, “On the effective thermal conductivity of wetted zeolite under the working conditions of an adsorption chiller,” *Appl. Therm. Eng.*, vol. 31, no. 14–15, pp. 2241–2246, 2011.

[39] Y. Y. Tanashev and Y. I. Aristov, “Thermal conductivity of a silica gel + calcium chloride system: The effect of adsorbed water,” *Inzhenerno-Fizicheskii Zhurnal*, vol. 73, no. 5, pp. 893–901, 2000.

[40] A. V. Luikov, A. G. Shashkov, L. L. Vasiliev, and Y. E. Fraiman, “Thermal conductivity of porous systems,” *Int. J. Heat Mass Transf.*, vol. 11, no. 2, pp. 117–140, Feb. 1968.

[41] H. Bjurström, E. Karawacki, and B. Carlsson, “Thermal conductivity of a microporous particulate medium: moist silica gel,” *Int. J. Heat Mass Transf.*, vol. 27, no. 11, pp. 2025–2036, 1984.

[42] M. Bahrami, M. M. Yovanovich, and J. R. Culham, “Effective thermal conductivity of rough spherical packed beds,” *Int. J. Heat Mass Transf.*, vol. 49, no. 19–20, pp. 3691–3701, Sep. 2006.

[43] E. Tsotsas and H. Martin, “Thermal conductivity of packed beds: A review,” *Chem. Eng. Process.*, vol. 22, no. 1, pp. 19–37, Jul. 1987.

[44] M. M. Yovanovich and E. E. Marotta, “Heat Transfer Handbook - Thermal Spreading and Contact,” *Heat Transf. Handb.*, 2003.

[45] K. Fayazmanesh, S. Salari, and M. Bahrami, “Effective thermal conductivity modeling of consolidated sorption composites containing graphite flakes,” *Int. J. Heat Mass Transf.*, vol. 115, pp. 73–79, Dec. 2017.

[46] E. Pop, V. Varshney, and A. K. Roy, “Thermal properties of graphene: Fundamentals and applications,” *MRS Bull.*, vol. 37, no. 12, pp. 1273–1281, Nov. 2012.

[47] Imerys, “TIMREX® C-THERM^{TM} 002 - Imerys - datasheet,” Jul-2020. [Online]. Available: https://polymer-additives.specialchem.com/product/a-imerys-timrex-c-therm-002. [Accessed: 11-Apr-2021].

[48] M. Bahrami, M. M. Yovanovich, and J. R. Culham, “Thermal joint resistances of nonconforming rough surfaces with gas-filled gaps,” *J. Thermophys. Heat Transf.*, vol. 18, no. 3, pp. 326–332, 2004.

[49] M. Bahrami, M. M. Yovanovich, and J. R. Culham, “Thermal joint resistances of conforming rough surfaces with gas-filled gaps,” *J. Thermophys. Heat Transf.*, vol. 18, no. 3, pp. 318–325, May 2004.

[50] M. R. Conde, “Properties of aqueous solutions of lithium and calcium chlorides: Formulations for use in air conditioning equipment design,” *Int. J. Therm. Sci.*, vol.

43, no. 4, pp. 367–382, 2004.

[51] S. E. Gustafsson, “Transient plane source techniques for thermal conductivity and thermal diffusivity measurements of solid materials,” *Rev. Sci. Instrum.*, vol. 62, no. 3, pp. 797–804, Mar. 1991.

[52] M. Cermak, “Natural graphite sheet heat sinks for power electronics,” Simon Fraser University, 2020.

[53] H. D. Ab, “Hot Disk Thermal Constants Analyser Instruction Manual,” 2013.

Appendix A.

MATLAB code for analytical model

The MATLAB code presented in this section is used to analytically model the thermal resistance network to predict the effective thermal conductivity and diffusivity of sorbent composites.

```
clear all;

clc;

%% Thermal Conductivity

Ks = 1.35; %(W/m.K) %Thermal conductivity of solid Silica

Kw = 0.6; %(W/m.K) %Thermal conductivity of salt solution

K_p = 8; %(W/m.K) %Thermal conductivity of Additive


%% Density:

Pho_s = 2400; %Kg/m3 Silica Gel True Density

Pho_sg = 654; %Kg/m3 Silica Gel Bulk Density

Pho_w = 1000; %Kg/m3 Water Density

Pho_p = 640; %Kg/m3 GF Bulk Density


%% Specific Heat Capacity

cpw = 4184; %J/kg.K

cps = 1000; %J/kg.K
```

```
cpg = 720; %J/kg.K


%% Porosity:

Porosity_0 = 70; %Porosity percentage


%% Geometry

dps = 16.76; %nm Average Pore Diameter

dpc = 2^(-1/3)*3^(1/6)*pi^(1/3)*dps; %Equivalent Cubic Diagonal

L = dpc*3^(-1/2);

PP = [12*pi*3^(1/2)*(1/dpc)^3  -9*pi*(1/dpc)^2   0   1-Porosity_0/100];

rs_roots = roots(PP);

rs = rs_roots(rs_roots<L/2 & rs_roots>0); %Host matrix radius


omega_array = [0.02 0.2 0.5 0.7]; %Uptake

for i = 1:4

omega = omega_array(i);

QQ = [-1  3*dpc/(4*3^(1/2))-3*rs   3*dpc*rs/(2*3^(1/2))   -(omega*((3*dpc/(4*3^(1/2))-
rs))*rs^2*Pho_s)/Pho_w];

tw_roots = roots(QQ);

tw(i)=tw_roots(tw_roots<(L/2) & tw_roots>0); %uptake thickness

end
```

```
ls = L-2*rs;

z = length(tw);

for j=1:z

rw(j) = rs+tw(j);

lw = L-2*rw;


%% Resistances

R_sL = (4*L)/(Ks*pi*(rs^2)/2);

R_wls(j) = 8*ls/(Kw*pi*(rw(j)^2-rs^2));

syms x;

R_sw = int(sin(x)/(Ks*sin(x)+Kw*(1-sin(x))), 0, pi/2);

R_swrs(j) = (1/tw(j))*sym2poly(R_sw);

R1(j) = 2*R_swrs(j) + R_wls(j);


%% Final R and K:

R(j) = 1/(1/R_sL + 1/R1(j) + 1/R1(j));

K_m(j) = (4/(R(j)*L)); %Thermal conductivity of effective medium


%% Volumes:

Vs = (L+2*ls)*(pi*rs^2)/4;

Vw(j) = (L+2*lw(j))*(pi/4)*(rw(j)^2-rs^2);
```

```
Vg = (L^3/4)-Vs;

%% Mass, combined density and combined cp

mw(j) = Pho_w*Vw(j);

ms = Pho_s*Vs;

mT(j) = mw(j)+ms;

Pho_T(j) = (mw(j)+ms)/(L^3/4);

cpT(j) = (ms/mT(j))*cps+(mw(j)/mT(j))*cpw;


%% Additive Particle

%Geometry:

rp = 544;

t = 4.3;

a = 1100;

w = 5.5:0.5:500;

n = length(w);

for i = 1:n

%Volume Fraction

Vm(i) = a*a*w(i);

Vp = t*pi*rp^2;

VF(i) = Vp/Vm(i);

wt(i) = 100*(Vp*Pho_p)/(Vm(i)*Pho_s);
```

```
%Horizontal:

K_h(i,j) = (w(i)*K_m(j)*(K_m(j)*(a^2-pi*rp^2)+K_p*pi*rp^2))/((w(i)-t)*((a^2-
pi*rp^2)*K_m(j)+K_p*pi*rp^2)+t*a^2*K_m(j));

%Vertical:

R_4(j) = int(sin(x)/(K_p*t*sin(x)+K_m(j)*t*(1-sin(x))), 0, pi/2);

R4(j) = sym2poly(R_4(j));

R5(j) = (4*rp)/(K_m(j)*t*(a-2*rp));

R6(j) = (a-2*rp)/(2*K_m(j)*a*t);

R7(i,j) = 2/(K_m(j)*(w(i)-t));

K_v(i,j) =
((R4(j)*R5(j))/(2*R4(j)+R5(j))+2*R6(j)+R7(i,j)/2)/(w(i)*(R7(i,j)/2)*((R4(j)*R5(j))/(2*R4(j)+R5
(j))+2*R6(j)));


Keff(i,j) = (cos(45)^2)*K_v(i,j)+(sin(45)^2)*K_h(i,j); %Effective thermal conductivity of
consolidated sorbent composite


mm(i,j) = Pho_T(j)*(Vm(i)-Vp);

mp = Pho_p*Vp;

mF(i,j) = mm(i,j)+mp;

Pho_F(i,j) = (mm(i,j)+mp)/(Vm(i));

cpF(i,j) = (mp/mF(i,j))*cpg+(mm(i,j)/mF(i,j))*cpT(j);
```

```
Alpha(i,j) = Keff(i,j)/(Pho_F(i,j)*cpF(i,j)); %Effective thermal diffusivity of consolidated
sorbent composite

end

end


%% Results

plot(wt,Keff(:,1),wt,Keff(:,2),wt,Keff(:,3),wt,Keff(:,4));

pbaspect([1 1 1]);

xlabel('Graphite Flakes Content (wt. %)');

ylabel('Thermal Conductivity (W/m.K)');

xlim([0 16]);
```

Appendix B.

Thermal properties measurements

Table A.1. Thermal conductivity measurements data with TPS for the consolidated sorbent composites CG0, CGF5, CGF10, CGF15. Samples were measured at 2, 20, 50 and 70% RH.

Additive content:	Thermal conductivity ($W \cdot m^{-1} \cdot K^{-1}$)			
	RH: 2%	RH: 20%	RH: 50%	RH: 70%
φ=0%	0.11	0.15	0.27	0.31
φ=5%	0.24	0.36	0.47	0.55
φ=10%	0.47	0.60	0.74	0.87
φ=15%	0.70	0.95	1.14	1.31

Table A.2. Thermal conductivity measurements data with TPS for the consolidated sorbent composites CG0, CENG1, CENG3, CENG5. Samples were measured at 2, 20, 50 and 70% RH.

Additive content:	Thermal conductivity ($W \cdot m^{-1} \cdot K^{-1}$)			
	RH: 2%	RH: 20%	RH: 50%	RH: 70%
φ=0%	0.11	0.15	0.27	0.31
φ=1%	0.22	0.28	0.35	0.44
φ=3%	0.43	0.49	0.56	0.67
φ=5%	0.74	0.8	0.85	0.99

Table A.3. Thermal diffusivity measurements data with TPS for the consolidated sorbent composites CG0, CGF5, CGF10, CGF15. Samples were measured at 2, 20, 50 and 70% RH.

Additive content:	Thermal diffusivity ($m^2 \cdot s^{-1}$)			
	RH: 2%	RH: 20%	RH: 50%	RH: 70%
φ=0%	1.15E-07	1.18E-07	1.20E-07	1.27E-07
φ=5%	2.40E-07	2.50E-07	3.00E-07	3.70E-07
φ=10%	4.80E-07	5.10E-07	6.10E-07	7.30E-07
φ=15%	9.00E-07	1.00E-06	1.10E-06	1.20E-06